



HAL
open science

Mutation-Specific Guide RNA for Compound Heterozygous Porphyria On-target Scarless Correction by CRISPR/Cas9 in Stem Cells

Florence Prat, Jérôme Toutain, Julian Boutin, Samuel Amintas, Grégoire Cullot, Magalie Lalanne, Isabelle Lamrissi-Garcia, Isabelle Moranvillier, Emmanuel Richard, Jean-Marc Blouin, et al.

► To cite this version:

Florence Prat, Jérôme Toutain, Julian Boutin, Samuel Amintas, Grégoire Cullot, et al.. Mutation-Specific Guide RNA for Compound Heterozygous Porphyria On-target Scarless Correction by CRISPR/Cas9 in Stem Cells. Stem Cell Reports, 2020, 15, pp.677 - 693. 10.1016/j.stemcr.2020.07.015 . hal-03492339

HAL Id: hal-03492339

<https://hal.science/hal-03492339>

Submitted on 9 Sep 2022

HAL is a multi-disciplinary open access archive for the deposit and dissemination of scientific research documents, whether they are published or not. The documents may come from teaching and research institutions in France or abroad, or from public or private research centers.

L'archive ouverte pluridisciplinaire **HAL**, est destinée au dépôt et à la diffusion de documents scientifiques de niveau recherche, publiés ou non, émanant des établissements d'enseignement et de recherche français ou étrangers, des laboratoires publics ou privés.



Distributed under a Creative Commons Attribution - NonCommercial 4.0 International License

Mutation-specific guide-RNA for compound

heterozygous porphyria on-target scar-less

correction by CRISPR-Cas9 in stem cells

Authors:

Florence Prat^{1,2}, Jérôme Toutain⁴, Julian Boutin^{1,2}, Samuel Amintas^{1,2,6}, Grégoire Cullot^{1,2},
Magalie Lalanne^{1,2}, Isabelle Lamrissi-Garcia^{1,2}, Isabelle Moranvillier¹, Emmanuel
Richard^{1,2,3,5}, Jean-Marc Blouin^{1,2,3,5}, Sandrine Dabernat^{1,2,3,5}, François Moreau-Gaudry^{1,2,3,5#}
et Aurélie Bedel^{1,2,3,5#}

¹Univ Bordeaux, 33000 Bordeaux France. ²INSERM U1035, Biotherapy of genetic diseases, inflammatory disorders and cancers, 33000 Bordeaux, France. ³Biochemistry Laboratory, CHU Bordeaux, 33000 Bordeaux, France. ⁴Medical genetic laboratory, CHU Bordeaux, 33000 Bordeaux, France. ⁵Laboratory of excellence, GR-Ex, Imagine institute, 75015 Paris, France, ⁶Laboratory of Tumor Biology, CHU Bordeaux, 33604 Pessac France. #equal contribution

Contact information: aurelie.bedel@u-bordeaux.fr

Running title: Compound heterozygous mutation perfect correction

Keywords: CRISPR-Cas9, gene therapy, iPSC, precise genome editing, Congenital Erythropoietic Porphyria, compound heterozygous recessive disease, mutation specific.

Summary:

CRISPR-Cas9 is a promising technology for gene correction. However, the edition is often biallelic, and uncontrolled small insertions and deletions (indels) concomitant to precise correction are created. Mutation-specific guide-RNAs were recently tested to correct dominant inherited diseases, sparing the wild-type allele. We tested an original approach to correct compound heterozygous recessive mutations. We compared editing efficiency and genotoxicity by biallelic guide-RNA *versus* mutant allele-specific guide-RNA in iPSCs derived from a congenital erythropoietic porphyria patient carrying compound heterozygous mutations resulting in *UROS* gene invalidation. We obtained UROS function rescue and metabolic correction with both guides with the potential of use for porphyria clinical intervention. However, unlike the biallelic one, the mutant allele-specific guide was free of on-target collateral damages. We recommend this design to avoid genotoxicity and to obtain on-target scar-less gene correction for recessive disease with frequent case of compound heterozygous mutations.

Introduction:

Congenital Erythropoietic Porphyria (CEP) is an autosomal recessive disorder due to a profound deficiency in the enzymatic activity of uroporphyrinogen III synthase (UROS; EC 4.2.1.75), the fourth enzyme of the heme biosynthetic pathway (Richard et al., 2008; Ged et al., 2009; Erwin and Desnick, 2019). This defect leads to the accumulation of the fluorescent type-I porphyrin isomers, causing dermatological lesions and hemolytic anemia. The clinical severity of the disease and the lack of specific treatment, besides bone marrow (BM) transplantation (Lagarde et al., 1998; Tezcan et al., 1998; Peinado et al., 2013; Thomas et al., 1996; Shaw et al., 2001; Harada et al., 2001), are strong arguments for gene therapy (Richard et al., 2008). Additive gene therapies are successful in treating monogenic hematopoietic disorders (Fischer et al., 2015; Ribeil et al., 2017; Morris et al., 2017). We and others (Bishop

et al., 2006; Ged et al., 2006; Yasuda and Desnick, 2019), have generated an animal model of CEP (*Uros*^{c.744C>A/c.744C>A}-knock-in mice (p.Pro248Gln)) to evaluate the efficacy of gene therapy. Lentiviral additive gene therapy with *UROS* cDNA into hematopoietic stem cells (HSCs) resulted in the complete and long-term enzymatic, metabolic, and phenotypic correction of the disease, with a better survival of the corrected red blood cells (Robert-Richard et al., 2008). This data was a proof of concept of a successful gene therapy for this disease. However, reports of proviral insertional leukemogenesis (Hacein-Bey-Abina et al., 2008) underscore the need for safer methods. The discovery of key transcription factors enabling reprogramming of a somatic cell into a pluripotent stem cell, called an induced pluripotent stem cell (iPSC)(Takahashi et al., 2007), has provoked an exciting rebound in gene-therapy research. Indeed, these cells allow clonal selection of corrected cells with safe provirus integration and further expansion for autologous graft.

We successfully performed additive lentiviral gene therapy in hiPSC (human iPSC) from a CEP-patient without risk of insertional oncogenesis by selection of corrected hiPSC clones with only one integration in a genomic safe harbor (Bedel et al., 2012).

However, exogenous sequence integration in the genome may carry unknown side effect and the inserted transgene is under the control of a non-physiological promotor. The CRISPR-Cas9 system is a seducing alternative to additive gene therapy (Doudna and Charpentier, 2014). Editing a gene at its endogenous locus by removing or correcting deleterious mutations rather than adding a new transgene has the potential to solve insertional mutagenesis and non-physiological gene regulation (Cong et al., 2013; Kohn and Kuo, 2017). CRISPR-Cas9 is an RNA-guided DNA endonuclease system targeting a specific genomic sequence complementary to a single-guide-RNA (sgRNA)(Cong et al., 2013; Doudna and Charpentier, 2014; Hsu et al., 2013; Jinek et al., 2012). Most publications report the use of engineered Cas9-nucleases to invalidate genes. Cas9 produces DSBs at sites of interest mainly solved by

error-prone non-conservative non-homologous end-joining (NHEJ) repair pathway that introduces insertions and deletions (indels) leading to disrupted targeted sequence (Boch et al., 2009; Porteus and Baltimore, 2003; Zhang et al., 2011). It is also possible to edit genes by homology direct repair (HDR) if a DNA template is provided (Yang et al., 2014). However, simultaneous to HDR, NHEJ occurs (Liu et al., 2019). The on-target NHEJ activated in response to DNA DSBs has often been underestimated. Precise genome editing (PGE) ratio measures needed HDR versus competitive unwanted indels. For example, in the CEP model and for *UROS* target, we recently demonstrated that uncontrolled DNA sequence modifications induced by the NHEJ are very frequent in HEK-293T, with a PGE ratio at 0.53 (Cullot et al., 2019). In any on-target site, repair introducing indels is twice as frequent as precise HDR. This PGE ratio is even lower in hiPSC (Li et al., 2018; Liang et al., 2017). This underlines the need to find new tools to improve PGE ratio.

Several approaches have been proposed in order to improve the PGE ratio. It is possible to insert a positive selection cassette in the donor template. However, this carries a genotoxic risk by transgene integration and is susceptible to immune response against the exogenous protein. Other techniques have been described such as the inhibition of NHEJ by suppressing DNA ligase IV (Hu et al., 2018b; Maruyama et al., 2015), KU70 (Chu et al., 2015), 53BP1 (Canny et al., 2018; Jayavaradhan et al., 2019; Nambiar et al., 2019) and polymerase Θ (Saito et al., 2017; Zelensky et al., 2017); alternatively, HDR activation by the use of RAD51 agonist (Song et al., 2016) or synchronizing the cells in S-G2 phases (Zhang et al., 2017; Janssen et al., 2019) promote HDR.

Interestingly, it is also possible to play on the design of the guide RNA (gRNA). Indeed, a mutant allele-specific gRNA invalidated only mutant alleles in dominant diseases *in vitro* (Monteys et al., 2017; Yamamoto et al., 2017; Burnight et al., 2017; Giannelli et al., 2018)

and *in vivo* (Xie et al., 2016). This approach was used to correct a dominant mutant allele using a template with (Smith et al., 2015) or without (Rabai et al., 2019) a selection cassette.

We hypothesized that a mutant allele-specific gRNA could be precisely corrected by HDR in recessive diseases with compound heterozygous mutations. Avoiding DSB in the WT allele is the only way to prevent Indels, preserving wild-type (WT) allele integrity and obtaining a perfect PGE ratio.

In this work, we propose to correct hiPSC derived from a CEP patient carrying two heterozygous mutations for the *UROS* gene by genome editing using CRISPR-Cas9. We compared editing efficiency and genotoxicity by biallelic guide-RNA *versus* mutant allele-specific guide-RNA. We showed that a mutant allele-specific guide was mandatory to perfectly correct cells without on-target indels and obtain efficient correction of CEP recessive disease with compound heterozygous mutations, interesting for future clinical applications.

Results

CEP-hiPSC characterization

To evaluate the mutant allele-specific approach to correct CEP, we used hiPSCs previously reprogrammed from a CEP-patient keratinocytes in our lab (Bedel et al., 2012). After cell expansion, the genotype was confirmed by PCR and Sanger sequencing (Figure 1A). The patient is a compound heterozygous for the *UROS* gene with one mutation in the exon 4 (c.217C>T) and another in the exon 10 (c.683C>T). Although these combined mutations lead to a dramatic decrease of the URO-synthase (URO-S) enzymatic activity 0.15 ± 0.07 vs 19.3 ± 1.7 for WT cells, n=3 (Figure 1B), CEP-hiPSCs do not spontaneously accumulate type-I porphyrins detectable by flow cytometry (Figure 1C left). By contrast, the exposure to the

heme biosynthesis precursor (δ -amino-levulinic acid (ALA)) induced specific fluorocytes appearance due to type-I porphyrins accumulation in the mutated cells (Figure 1C right).

Correction of the *UROS* mutations comparing two gRNA design strategy

We aimed to compare the efficacy of the mutant allele-specific gRNA approach to a classic biallelic gRNA. We designed a biallelic gRNA-10 for exon 10, targeting both alleles (mutant and WT), close to the c.683C>T mutation (Figure 1D and 2A). For the exon 4, the gRNA-4 includes the mutation c.217C>T and is mutant allele-specific (Figure 1D and 5A).

Because editing is low in primary stem cells, we designed tools allowing transfected cells sorting, using two plasmids expressing Cas9-ZsGreen or the gRNA, with fluorescent Alexa 647-ssODN HDR templates (75 or 80bp). These templates bear silent mutations introducing restriction sites allowing HDR quantification by Restriction Fragment Length Polymorphism (RFLP) (Figure 1D). Indels and HDR rates were confirmed by sequencing and ICE/TIDER software analyses. We characterized enzymatic and metabolic activities of the corrected cells and their subclones (*UROS* enzymatic activity rescue, porphyrins disappearance) (Figure 1D).

Biallelic gRNA for exon 10 *UROS* editing

After transfection with the Cas9-ZsGreen, gRNA-10 plasmids and the 75nt-ssODN-A647 template, cells were sorted for ZsGreen and Alexa Fluor 647 staining (Figure 2A and 2B). Sanger sequencing revealed Indels from cut site indicating a DSB. This result was confirmed by ICE and TIDER analyses (83% of Indels) (Figure 2B, Figure S1A left). These techniques also indicated 2% of HDR, which is confirmed by RFLP (2.8% of alleles with *ApaI* site), showing a low frequency of precise editing (Figure 2B).

To sort the corrected cells, which no longer accumulate fluorescent porphyrins, we exposed the cells to ALA, and sorted the non-fluorescent cells (PE-Cy5 negative = porphyrin negative) (Figure 3A). As expected in the non-fluorescent cells, the mutated T reverted to C, and the

two expected silent mutations (*ApaI*) were introduced. HDR was quantified by ICE (38%), TIDER (22%) and confirmed by RFLP (41%) (Figure 3A and Figure S1A right). These data suggest that only one of the two alleles was edited by HDR in these corrected cells. We obtained a 24-fold increase of UROS activity compared to an isogenic CEP-hiPSC (3.65 ± 0.33 vs. 0.15 ± 0.07 for CEP-hiPSC before editing). This enzymatic rescue prevented porphyrins accumulation, but was partial compared to non-isogenic WT-hiPSC from a healthy patient (3.65 ± 0.33 vs 19.3 ± 1.7 U/mg prot for WT cells) (Figure 3B). However, Sanger sequence chromatogram and ICE/TIDER analyses revealed that this correction was concomitant with a high indels rate (53% and 23% respectively) (Figure 3A). These indels are two symmetric 25-base deletions in favor of MMEJ (Microhomology-Mediated End Joining) repair (Figure 3C). Most indels seemed to be the same deletion, due to clonal correction or clonal expansion of these corrected cells. Anyway, the PGE ratio (HDR/Indels) ranked between 0.7 or 0.9 with ICE or TIDER results, confirming the predominant NHEJ repair pathway. We then cultured corrected CEP-hiPSCs under clonal conditions in order to find one subclone perfectly corrected, without indels (HDR/WT or HDR/HDR). All six analyzed subclones contained the *ApaI* site and the corrected c.683C base, but also indels (Figure 4A), while URO-S enzymatic activity was restored as for the polyclonal cell population (3.8 ± 0.4 U/mg prot, n=6 clones) (Figure 4B). In conclusion, in all the analyzed corrected cells, both specific correction of the mutated allele and indels on the homologous allele occurred because the gRNA targeted both alleles.

Mutant allele specific-gRNA for exon 4 *UROS* editing

Unlike exon 10, we used a mutant allele-specific RNA guide (gRNA-4) that targeted only the mutated allele for the editing of exon 4 (Figure 5A). Using the same strategy, we transfected the CEP-hiPSCs with the ZsGreen-nuclease plasmid, the gRNA-4 plasmid with a ssODN template (80pb-ssODN-A647) bearing a silent mutation introducing a *SacI* restriction site

(Figure 5A). After sorting of the double positive ZsGreen⁺ / A647⁺ cells, we obtained corrected cells (4.7% by RFLP, 5% by deep sequencing, undetectable by ICE/TIDER analyses) (Figure 5B and Figure S1B left). As shown by Sanger sequencing, correction events were concomitant with indels, 37%, 33% and 30.9% by ICE, TIDER and deep sequencing analyses, respectively (Figure 5B and Figure S1B left). Indels sequences consisted in five short deletions (1 to 5 bases) and 1 base insertion (Figure 5C) probably due to NHEJ repair. We sorted, in presence of ALA, the porphyrin negative cells, supposedly the corrected cells. Sanger chromatogram confirmed a perfect mutation correction c.217T (Figure 6A). Molecular analysis confirmed C to T editing with a high HDR rate by ICE (70%), TIDER (45%), RFLP (39%) and deep sequencing (44.4%) (Figure 6A and Figure S1B right). Although no indel events were detectable on the chromatogram and by ICE/TIDER analyses (Figure 6A, 6B and Figure S1B right), deep sequencing revealed around 7% of alleles with indels, in the polyclonal mix. Cells demonstrated phenotypic correction with metabolic activity restoration by HPLC (3.54 ± 0.4 U/mg protein), corresponding to a 24-fold increase compared to the isogenic CEP-hiPSC (Figure 6C). To verify indels absence in the corrected cells, we cultured seven “porphyrin negative” subclones. Six out of the seven contained the corrected mutation and the *SacI* digestion site without indels (Figure 7A), resulting in a perfect PGE ratio. One was not corrected, but bared indels, probably because of imperfect cell sorting, and in agreement with deep sequencing results (7% of alleles with indels). The six corrected subclones restored URO-S metabolic activity (3.95 ± 0.3 U/mg protein, n=6) (Figure 7B) similar to the polyclonal cell population. Together these data showed similar enzymatic correction between *UROS* exon 10 and *UROS* exon 4 corrected cells, but without genotoxicity on the opposite allele thanks to a gRNA encompassing the mutation.

To check putative off-target damages by CRISPR-Cas9 nuclease and the gRNA-4, we quantified indels in the top 10 off-target sequences predicted by CRISPOR. We observed low

indel rates (7 and 5%) in only two of the top 10 ranked loci. The first one is located in an intronic region and the second one in an intergenic region (Figure S2). No off-target site is on chromosome 10 minimizing risks of internal chromosomal rearrangement.

We recently published that *UROS* exon 4 targeting by CRISPR-Cas9 nuclease in HEK293T could induce chromosome 10q terminal truncations, with megabase-scale deletion (Cullot et al., 2019). Thus, we evaluated genome integrity in exon 4 perfectly corrected CEP cells. We focused on the *UROS* locus (10q26.2) harbors in iPSC polyclonal population and subclones. We performed FISH analysis using probes framing *UROS* (a proximal probe at 4.6 Mb upstream *UROS*, labeled in green (G), and a distal probe 4.4 Mb downstream *UROS*, labeled in orange (O)) (Figure 7C). Polyclonal analysis did not reveal loss of the orange probe, which would identify chromosomal end losses. All the subclones were 2O/2G (Figure 7C) suggesting the absence of megabase scale deletions and chromosome 10q terminal truncation. In the same way, none of the tested subclones lost orange signal (0/3 subclones). Additionally, we observed amplification of two alleles by Sanger sequences (heterozygous sequences, Figure 7A), suggesting the correct integrity of the diploid clones, without kilobase deletions. To confirm the absence of Cas9-induced chromosomal instability, we performed karyotype analysis after three rounds of Cas9 nuclease nucleofections with the gRNA-4. We did not observe any chromosome abnormality after editing (mitosis with one X-chromosome deletion were already present) (Figure S3).

Collectively, these data suggest that the use of a mutant allele-specific gRNA approach to edit exon 4 produced a clean and efficient correction of *UROS* in human iPSCs, with a perfect PGE ratio. (Figure 7D).

Discussion

Here, we succeeded in targeting and correcting by HDR the mutant alleles (in exon 4 and exon 10 of the *UROS* gene) of a compound heterozygous CEP patient hiPSC. To evaluate the genomic correction, we used deep-sequencing and ICE/TIDER softwares that compared Sanger chromatograms. Generally, we obtained good correlations between them and the gold standard deep-sequencing. However, low HDR rates are not detected by software analyses (<5%) and we observed some discrepancies between these two softwares results. So, this interesting tools, easy-to-use and costless, need to be used with precaution for precise quantification.

We obtained full metabolic correction of CEP-hiPSCs by CRISPR-Cas9, by both guides design, with disappearance of porphyrin accumulation. Correction of one mutation, either in exon 4 or in exon 10, led to the same partial URO-S enzymatic rescue. Intriguingly, monoallelic corrections did not restore half of regular hiPSC URO-S enzymatic activity, with two WT alleles, probably because they are not isogenic and heterogeneity between clones is high. As URO-S activity is partially restored by both approaches (mutant allele-specific or biallelic), they could be considered equivalent editing. However, in mammalian cells, DSBs are predominantly repaired by NHEJ, while HDR is less active (Chu et al., 2015; Li et al., 2018; Liang et al., 2017). In our work, the first correction design consisted in routine approach, targeting the *UROS* exon 10 by a biallelic targeting gRNA complementary to a sequence next to the mutation. This always resulted in undesired indels in the WT allele in parallel to correct editing of the other allele. This observation relates to the experimental difficulty in generating specific heterozygous mutations at the cellular level since most CRISPR-Cas9 editing events are biallelic (Wang et al., 2013). The PGE ratio achieved in hiPSCs was the same than in the HEK-293T cells (Cullot et al., 2019), with indels twice as frequent as precise correction. Besides inducing gene KO, on-target indels could lead to the production of abnormal proteins with immunogenic properties, or potentially pathogenic by

gain of function. Indeed, mutations in coding regions can promote abnormal interactions, alter the interaction of the mutant protein with its natural binders and/or promote misfolding/aggregation (Li et al., 2019).

The second correction strategy to achieve allele specificity while not impacting the WT allele, designed a guide sequence encompassing the mutation site. Together with the hiPSC-clonal approach, this design produced scar-less editing, without undesired on-target indels and limited potential genotoxicity induced by CRISPR-Cas9 nuclease. Usually, gRNA of endonucleases, such as *Streptococcus pyogenes* Cas9 (SpCas9) and *Staphylococcus aureus* (SaCas9), can tolerate mismatches between gRNA and target DNA. In our study, we designed a mutant-specific guide with mutation next to the PAM (Protospacer Adjacent Motif) because this location do not accept mismatch (Hsu et al., 2013). So, we drastically spared the WT allele. It would not be the case if the mutation was in the guide but far from the PAM. In this case, guide would be permissive to this mutation, and would cut the WT allele too. This is in agreement with the fact that the CRISPR-Cas system can be a highly specific genome editing tool capable of distinguishing alleles differing by a single nucleotide, when this difference is in the seed sequence (Slaymaker et al., 2016).

To our knowledge, this is the first report of a CEP-hiPSC correction by CRISPR-Cas9 but, also the first allele-specific correction of a compound heterozygote for a recessive disease. Mutant allele-specific gRNA was already reported to target heterozygous mutation for indels-mediated inactivation in three autosomal dominant diseases *in vitro* (Monteys et al., 2017; Yamamoto et al., 2017) and *in vivo* (György et al., 2019; Monteys et al., 2017; Xie et al., 2016). Very recently, Rabai et al. showed elegant editing by HDR of *DNM2* using an allele-specific guide, but for the autosomal dominant form of centronuclear myopathy (Rabai et al., 2019). Importantly, in patients with rare recessive diseases, compound heterozygosity of pathogenic mutations is the most likely inheritance model if the parents are non-

consanguineous (Kamphans et al., 2013). In this situation, allele specific correction may be the most suitable approach. To this end, the Pollard lab developed a new software, AlleleAnalyzer, to facilitate allele specific gRNA design (Keough et al., 2019).

Despite high versatility and efficacy, the CRISPR-Cas9 nuclease tool has still limitations. First, there is bears a risk of off-target effects. The allele-specific guide design has no impact on putative off-target risk. In our model, we observed low percentages of indels in off-target sequences. This flaw could be solved by the new generation higher fidelity Cas (eSpCas9, spCas9-HF1, HypaCas9 (Ikeda et al., 2019)). For example, HypaCas9 enabled the discrimination of single-nucleotide polymorphisms (SNPs) and the introduction of monoallelic mutations in mouse zygotes (Ikeda et al., 2019). Second, on-target genotoxicity due to DSB was recently described. CRISPR-Cas9 can promote large deletions from few kilobases (Adikusuma et al., 2018; Kosicki et al., 2018; Shin et al., 2017) to many megabases (Cullot et al., 2019) after only one cut. These losses cause loss of heterozygosity (LOH). In the case of CEP-hiPSC, we did not observe any kilobase or megabase-scale deletions by FISH or PCR. We cannot exclude rare genomic abnormalities (below FISH limit of detection) or a distinct locus genotoxicity. Arthur R. Gorter de Vries *et al.*, recently alerted to LOH risk not by loss of genetic material but by replacement of the targeted sequence by a copy of the opposite allele. They observed this risk using an allele specific genome editing in diploid yeast, repaired by the break induced repair (BIR) mechanism (Gorter de Vries et al., 2019). Ma *et al.* confirmed this risk in human embryos (Ma et al., 2017). In our case, all subclones had the restriction site integration, demonstrating that the reparation mechanism involved the template by HDR and not the other homolog chromosome by BIR. Anyway, clonal approach of hiPSC renders careful selection of cells with genomic integrity and scar-less editing possible.

The heterozygous composite proportion in patients with recessive diseases is frequent (phenylketonuria, Tay Sachs...). For example, for cystic fibrosis, which is the more prevalent genetic disease, this proportion is 40%. In these cases, the mutant allele-specific guide approach is the best way to avoid undesired WT allele uncontrolled editing and on-target side effects due to the risk of the production of abnormal protein. The fact that the PAM should be localized near the heterozygous mutation may be solved by new generation Cas9 tools such as the xCas9 with broad PAM eligibility (Hu et al., 2018a). Since unwanted indels are caused by DSB, another solution could be an editing without DSB with the recent prime-editor (Anzalone et al., 2019) or the base editors systems (Molla and Yang, 2019). Indeed, c.217T>C is eligible to CBE base editor. However, their efficacy and specificity in hiPSC have still to be improved.

Experimental procedures

Cell culture and transfection.

Induced pluripotent stem cells from CEP patient and WT individual were previously described (Bedel et al., 2012) and obtained after informed consent in accordance with the ethical standards of the responsible committee on human experimentation (Centre Hospitalier Universitaire de Bordeaux). Human iPSC clones were maintained as undifferentiated cells in cocultures with mitomycin MEFs. The ES medium used was the following: KO-DMEM (Invitrogen, Villebon sur Yvette, France) containing 20% KOSR (Invitrogen) (vol/vol), 10 ng/ml human bFGF (PeproTech), 1 mM GlutaMAX (Invitrogen), 100 mM Non-Essential Amino Acids (Invitrogen), 100 mM 2-mercaptoethanol (Sigma-Aldrich, Saint Louis, MO, USA), 50 mg/ml ascorbic acid (Sigma-Aldrich), 0.5 mM sodium butyrate (Sigma-Aldrich), 50 U/ml penicillin, and 50 mg/ml streptomycin (Invitrogen). The ES medium was changed every day. hiPSC subclones were cultured onto feeder-free Cellartis® DEF-CS™ Culture System

(Takara Bio Europe), therefore exhibiting proliferation as monolayer hiPSC lines with continuous passaging twice a week, as previously described(Asplund et al., 2016).

Editing tools.

Cells were transfected by electroporation using the Nucleofector AMAXA 4D electroporation system (Lonza®, Bale, Switzerland), using P3 primary cell kit and CB-150 program. In brief, 800 000 cells were nucleofected with 20 µg of nuclease containing plasmid, 20µg gRNA containing plasmid, and 1.7 µM of specified ssODN. Cells were then seeded onto 12-well plates (Corning®, Tewksbury, MA, USA) and cultured as described above. Transfected cells were then positively selected 24 h after transfection by ZsGreen-positive and A647-positive selection by Fluorescent activating cellsorting (FACS) using BD FACS Aria®.

The nuclease-containing plasmid was a modified version of lentiCRISPRv2 obtained from Addgene (Cambridge, MA, USA) (#52961). The ZsGreen sequence was inserted by digesting the lentiCRISPRv2 by BamHI-SacII (New England Biolabs, Ipswich, MA, USA) and replaced this fragment by a BamHI-P2A-ZsGreen-WPRE sequence synthesized by Eurofins Genomics (Germany).

All sgRNAs were designed using the CHOPCHOPv2 algorithm⁶⁸ (chopchop.cbu.uib.no) and based on a unique sequence with 20 nucleotides. All ssODN templates used in the study were purchased from Integrated DNA Technologies (IDT, Coralville, IA, USA). For 80nt-ssODN-A647 and 75nt-ssODN-A647, an Alexa Fluor® 647 was chemically linked at the 5' terminal end to ssODN by NHS Ester link (Supplementary table 1).

Flow cytometry for porphyrin accumulation.

UV-sensitive type-I porphyrins were excited at 496 nm and the emitted wavelength was approximately 667 nm, detected by the PE-Cy5-A PMT channel (FACSCanto, BD, Franklin Lakes, NJ, USA). Cells were sorted by BD FACS Aria®.

Sanger sequence and ICE analysis for allelic outcomes.

Genomic DNA was extracted using Nucleospin®Tissue (Macherey-Nagel, Duren, Germany) according to the manufacturer's protocol. The genomic region flanking UROS exon 4 (or exon 10) was amplified by PCR (HotStarTaq Plus DNA polymerase, Qiagen®, Venlo, Netherlands) with adequate primers (Supplementary Table 2). PCR products were purified with Nucleospin® Gel and PCR Clean-up (Macherey-Nagel). Sanger sequence was performed by Eurofins genomics®. Inference of CRISPR edit (ICE) and TIDER (Brinkman et al., 2018) (Tracking of Insertions, DEletions and Recombination events) were used to determine HDR and indels frequencies. PCR product from non-transfected CEP-hiPSC was provided as control chromatogram.

NGS-deep sequencing for allelic outcomes.

Genomic DNA was extracted using Nucleospin® Tissue (Macherey-Nagel®) according to the manufacturer's protocol. The genomic region flanking UROS exon4 was amplified by PCR (KAPA HiFi DNA polymerase, Kapa Biosystems®, CapeTown, South Africa) with adequate primers (Supplementary Table 1). PCR products were purified with Nucleospin® Gel and PCR Clean-up (Macherey-Nagel®). To prepare sequencing libraries, the Illumina Nextera XT Kit (Illumina®,San Diego, California, USA) was used and nested-PCR using Illumina primers was

performed on purified PCR products. An Illumina MiSeq instrument (Illumina®) was used for high-throughput sequencing. The average depth of each genome analysis was 30,000. Quality of paired-end reads was checked with FastQC (Galaxy,<https://usegalaxy.org/>). Then, quantification of HDR was performed on restriction site, and percentage of insertion and deletion and base rates were done at cut-site, using Alamut® Visual software.

Microhomology analysis.

The sequence around the gRNA-4 and gRN-10 target site of *UROS* exon 4 or 10 respectively, were uploaded to Microhomology-Predictor of CRISPR RGEN tools (<http://www.rgenome.net/mich-calculator/>) for microhomology sequence analysis. One of the 25-bp deletion for gRNA-10 has corresponding pattern scores of 114.7. The corresponding indel pattern was also identified by ICE analyze.

RFLP for HDR quantification.

UROS exon 4 or exon 10 PCR products were digested respectively with *SacI* or *ApaI* restriction enzyme (New England Biolabs, Ipswich, MA, USA) for 1 h at 37 °C. Then, 5 ng digestion products were loaded into the Agilent® 2200 TapeStation (Santa Clara, CA, USA) capillary electrophoresis using D1000 ScreenTape and D1000 reagents according to the manufacturer's protocol. Quality control of enzymatic digestion efficiency is included in each assay.

UROS enzymatic activity and metabolic correction.

UROS activity was determined by an enzyme-coupled assay as described previously (Tsai et al., 1987). Briefly, porphobilinogen was first converted to hydroxymethylbilane, the natural substrate for *UROS*, by hydroxymethylbilane synthase. Then, the uroporphyrinogen reaction

products were oxidized to their respective uroporphyrin isomers, which were then resolved and quantitated by reversed-phase high-pressure liquid chromatography. One unit was defined as the amount of enzyme that formed 1 nmol of uroporphyrinogen III per hour at 37 °C.

Off-target analysis.

For sgRNA targeting exon 4 *UROS* locus, the Top 10-predicted off-target sites, identified by CRISPOR software were amplified in genome-edited corrected CEP-hiPSC and subjected to Sanger sequencing, followed by comparison to non-transfected cells by ICE analysis.

Primers used for off-target analysis are in Supplementary Table 1.

Cytogenetic examination of chromosome 10.

FISH was performed on interphase nuclei, with probes targeting the locus 10q26.11 on chromosome 10: (BAC RP11–79M19probe, labeled in green) (Empire Genomics, Buffalo, NY, USA), and the locus 10q26.2 (BAC RP11–31M22 probe, labeled in orange) (Empire Genomics, Buffalo, NY,USA). Preparations were pre-treated as indicated below. Briefly, the slides were successively immersed in a 2x saline-sodium citrate buffer for 10 min at 37 °C, in a 0.01% pepsin solution for 10 min at 37 °C, in a 1x phosphate-buffered saline (PBS) solution for 5 minutes, in a 3.7% formaldehyde solution for 5 min, and in a 1xPBS solution for 5 minutes. FISH probes and DNA were then co-denatured according to the manufacturers' protocols, and hybridization was performed overnight at 37 °C. The slides were then successively immersed in wash solutions and the nucleic acids were counterstained by 4,6-diamidino-2-phenylindole. The slides were then placed under an Axio Imager2 microscope with an epi-fluorescence source (Carl Zeiss AG, Oberkochen, Germany). The microscope was linked to the Metafer4 software for automated image acquisition and processing

(MetaSystems GmbH, Altlußheim, Germany). Genomic DNA was extracted with the Wizard Kit (Promega Corporation, Madison, USA) following the protocol validated in the laboratory.

Karyotype.

After FrdU synchronization followed by a thymidine chase, standard R-banding analysis was performed on metaphase chromosomes obtained with all iPSC clones. At least 20 metaphase chromosomes were fully karyotyped.

Statistic.

Statistical significance was inferred when necessary. Graph Pad Prism 6 software was used for statistical analysis. Results are presented as mean \pm SEM (standard error of the mean). Shapiro-Wilkinson test was done to assess the normality distribution. When it was positive, the two-tailed unpaired t test was done to compare means of two groups and one-way ANOVA, completed with unprotected Fisher's Least Significant Difference test, was used to compare three groups. When normality distribution failed, non-parametric Kruskal Wallis was used. All comparisons are shown with black bars. Null hypothesis was rejected when p value < 0.05. *p < 0.05; **p < 0.01; ***p < 0.001; ns, non-significant.

Data Availability

All next-generation sequencing data sets have been deposited in the NCBI database under BioProject accession no. PRJNA645083 with associated BioSample no. SAMN15491845 for exon 4 of CEP-hiPSC non transfected, BioSample no. SAMN15491847 for transfected CEP-hiPSC with nuclease and RNA-guide plasmids and ssODN (Figure 5) and no. SAMN15491846 for corrected cells on exon 4 or porphyrines negative cells (Figure 6).

Acknowledgments

We thank Dr Feng Zhang for sharing plasmids through Addgene (Cambridge, MA, USA) and Vincent Pitard and Atika Zouine from the cytometry platform at Bordeaux University. This work was supported by the Association Française contre les Myopathies Grant # 20957, and the Agence de Biomédecine. We thank Florence Lichou, Beatrice Turcq and Nicolas Sevenet (Inserm U1218, Institut Bergonié, Bordeaux, France) for NGS analysis, and Valérie Prouzet-Mauléon for helpful CRISPR discussion. We thank Catherine Pain and Pr Alain Taieb for providing CEP patient keratinocytes (Bordeaux Hospital). We thank Katia Obama, Isabelle Lamy and Sandrine Hamon for administrative assistance and financial management.

Author contributions

F.P: Performing editing experiments and iPSC culture; G.C.: editing analysis; J.T., J.B.: FISH design and experiments; S.A.: deep-sequencing data analyses ; I.L.G: FACS analysis; M.L.: UROS enzymatic assay; I.M.: iPSC and MEF cell culture; J.M.B., E.Ri. and S.D: helpful discussion in the field of CRISPR/Cas9 and writing the manuscript; F.M.G. and A.Be: iPSC culture, design, analysis of data and writing the manuscript; funding acquisition, final approval of manuscript.

Declaration of interest: The authors have no conflict of interest

- Adikusuma, F., Piltz, S., Corbett, M.A., Turvey, M., McColl, S.R., Helbig, K.J., Beard, M.R., Hughes, J., Pomerantz, R.T., and Thomas, P.Q. (2018). Large deletions induced by Cas9 cleavage. *Nature* 560, E8–E9.
- Anzalone, A.V., Randolph, P.B., Davis, J.R., Sousa, A.A., Koblan, L.W., Levy, J.M., Chen, P.J., Wilson, C., Newby, G.A., Raguram, A., et al. (2019). Search-and-replace genome editing without double-strand breaks or donor DNA. *Nature* 576, 149–157.
- Asplund, A., Pradip, A., van Giezen, M., Aspegren, A., Choukair, H., Rehnström, M., Jacobsson, S., Ghosheh, N., El Hajjam, D., Holmgren, S., et al. (2016). One Standardized Differentiation Procedure Robustly Generates Homogenous Hepatocyte Cultures Displaying Metabolic Diversity from a Large Panel of Human Pluripotent Stem Cells. *Stem Cell Rev Rep* 12, 90–104.
- Bedel, A., Taillepierre, M., Guyonnet-Duperat, V., Lippert, E., Dubus, P., Dabernat, S., Mautuit, T., Cardinaud, B., Pain, C., Rousseau, B., et al. (2012). Metabolic Correction of Congenital Erythropoietic Porphyria with iPSCs Free of Reprogramming Factors. *The American Journal of Human Genetics* 91, 109–121.
- Bishop, D.F., Johansson, A., Phelps, R., Shady, A.A., Ramirez, M.C.M., Yasuda, M., Caro, A., and Desnick, R.J. (2006). Uroporphyrinogen III Synthase Knock-In Mice Have the Human Congenital Erythropoietic Porphyria Phenotype, Including the Characteristic Light-Induced Cutaneous Lesions. *The American Journal of Human Genetics* 78, 645–658.
- Boch, J., Scholze, H., Schornack, S., Landgraf, A., Hahn, S., Kay, S., Lahaye, T., Nickstadt, A., and Bonas, U. (2009). Breaking the Code of DNA Binding Specificity of TAL-Type III Effectors. *Science* 326, 1509–1512.
- Brinkman, E.K., Kousholt, A.N., Harmsen, T., Leemans, C., Chen, T., Jonkers, J., and van Steensel, B. (2018). Easy quantification of template-directed CRISPR/Cas9 editing. *Nucleic Acids Res* 46, e58–e58.
- Burnight, E.R., Gupta, M., Wiley, L.A., Anfinson, K.R., Tran, A., Triboulet, R., Hoffmann, J.M., Klaahsen, D.L., Andorf, J.L., Jiao, C., et al. (2017). Using CRISPR-Cas9 to Generate Gene-Corrected Autologous iPSCs for the Treatment of Inherited Retinal Degeneration. *Molecular Therapy* 25, 1999–2013.
- Canny, M.D., Moatti, N., Wan, L.C.K., Fradet-Turcotte, A., Krasner, D., Mateos-Gomez, P.A., Zimmermann, M., Orthwein, A., Juang, Y.-C., Zhang, W., et al. (2018). Inhibition of 53BP1 favors homology-dependent DNA repair and increases CRISPR–Cas9 genome-editing efficiency. *Nat Biotechnol* 36, 95–102.
- Chu, V.T., Weber, T., Wefers, B., Wurst, W., Sander, S., Rajewsky, K., and Kühn, R. (2015). Increasing the efficiency of homology-directed repair for CRISPR-Cas9-induced precise gene editing in mammalian cells. *Nat Biotechnol* 33, 543–548.
- Cong, L., Ran, F.A., Cox, D., Lin, S., Barretto, R., Habib, N., Hsu, P.D., Wu, X., Jiang, W., Marraffini, L.A., et al. (2013). Multiplex Genome Engineering Using CRISPR/Cas Systems. *Science* 339, 819–823.
- Cullot, G., Boutin, J., Toutain, J., Prat, F., Pennamen, P., Rooryck, C., Teichmann, M., Rousseau, E., Lamrissi-Garcia, I., Guyonnet-Duperat, V., et al. (2019). CRISPR-Cas9 genome editing induces megabase-scale chromosomal truncations. *Nature Communications* 10, 1136.
- Doudna, J.A., and Charpentier, E. (2014). The new frontier of genome engineering with CRISPR-Cas9. *Science* 346, 1258096.

- Erwin, A.L., and Desnick, R.J. (2019). Congenital erythropoietic porphyria: Recent advances. *Molecular Genetics and Metabolism* 128, 288–297.
- Fischer, A., Notarangelo, L.D., Neven, B., Cavazzana, M., and Puck, J.M. (2015). Severe combined immunodeficiencies and related disorders. *Nature Reviews Disease Primers* 1, 15061.
- Ged, C., Mendez, M., Robert, E., Lalanne, M., Lamrissi-Garcia, I., Costet, P., Daniel, J.Y., Dubus, P., Mazurier, F., Moreau-Gaudry, F., et al. (2006). A knock-in mouse model of congenital erythropoietic porphyria. *Genomics* 87, 84–92.
- Ged, C., Moreau-Gaudry, F., Richard, E., Robert-Richard, E., and de Verneuil, H. (2009). Congenital erythropoietic porphyria: mutation update and correlations between genotype and phenotype. *Cell. Mol. Biol. (Noisy-Le-Grand)* 55, 53–60.
- Giannelli, S.G., Luoni, M., Castoldi, V., Massimino, L., Cabassi, T., Angeloni, D., Demontis, G.C., Leocani, L., Andreazzoli, M., and Broccoli, V. (2018). Cas9/sgRNA selective targeting of the P23H Rhodopsin mutant allele for treating retinitis pigmentosa by intravitreal AAV9.PHP.B-based delivery. *Hum Mol Genet* 27, 761–779.
- Gorter de Vries, A.R., Couwenberg, L.G.F., van den Broek, M., de la Torre Cortés, P., ter Horst, J., Pronk, J.T., and Daran, J.-M.G. (2019). Allele-specific genome editing using CRISPR–Cas9 is associated with loss of heterozygosity in diploid yeast. *Nucleic Acids Res* 47, 1362–1372.
- György, B., Nist-Lund, C., Pan, B., Asai, Y., Karavitaki, K.D., Kleinstiver, B.P., Garcia, S.P., Zaborowski, M.P., Solanes, P., Spataro, S., et al. (2019). Allele-specific gene editing prevents deafness in a model of dominant progressive hearing loss. *Nat Med* 25, 1123–1130.
- Hacein-Bey-Abina, S., Garrigue, A., Wang, G.P., Soulier, J., Lim, A., Morillon, E., Clappier, E., Caccavelli, L., Delabesse, E., Beldjord, K., et al. (2008). Insertional oncogenesis in 4 patients after retrovirus-mediated gene therapy of SCID-X1. *J Clin Invest* 118, 3132–3142.
- Harada, F.A., Shwayder, T.A., Desnick, R.J., and Lim, H.W. (2001). Treatment of severe congenital erythropoietic porphyria by bone marrow transplantation. *Journal of the American Academy of Dermatology* 45, 279–282.
- Hsu, P.D., Scott, D.A., Weinstein, J.A., Ran, F.A., Konermann, S., Agarwala, V., Li, Y., Fine, E.J., Wu, X., Shalem, O., et al. (2013). DNA targeting specificity of RNA-guided Cas9 nucleases. *Nature Biotechnology* 31, 827–832.
- Hu, J.H., Miller, S.M., Geurts, M.H., Tang, W., Chen, L., Sun, N., Zeina, C.M., Gao, X., Rees, H.A., Lin, Z., et al. (2018a). Evolved Cas9 variants with broad PAM compatibility and high DNA specificity. *Nature* 556, 57–63.
- Hu, Z., Shi, Z., Guo, X., Jiang, B., Wang, G., Luo, D., Chen, Y., and Zhu, Y.-S. (2018b). Ligase IV inhibitor SCR7 enhances gene editing directed by CRISPR–Cas9 and ssODN in human cancer cells. *Cell Biosci* 8, 1–15.
- Ikeda, A., Fujii, W., Sugiura, K., and Naito, K. (2019). High-fidelity endonuclease variant HypaCas9 facilitates accurate allele-specific gene modification in mouse zygotes. *Communications Biology* 2, 1–7.

- Janssen, J.M., Chen, X., Liu, J., and Gonçalves, M.A.F.V. (2019). The Chromatin Structure of CRISPR-Cas9 Target DNA Controls the Balance between Mutagenic and Homology-Directed Gene-Editing Events. *Molecular Therapy - Nucleic Acids* 16, 141–154.
- Jayavaradhan, R., Pillis, D.M., Goodman, M., Zhang, F., Zhang, Y., Andreassen, P.R., and Malik, P. (2019). CRISPR-Cas9 fusion to dominant-negative 53BP1 enhances HDR and inhibits NHEJ specifically at Cas9 target sites. *Nature Communications* 10, 2866.
- Jinek, M., Chylinski, K., Fonfara, I., Hauer, M., Doudna, J.A., and Charpentier, E. (2012). A programmable dual RNA-guided DNA endonuclease in adaptive bacterial immunity. *Science* 337, 816–821.
- Kamphans, T., Sabri, P., Zhu, N., Heinrich, V., Mundlos, S., Robinson, P.N., Parkhomchuk, D., and Krawitz, P.M. (2013). Filtering for Compound Heterozygous Sequence Variants in Non-Consanguineous Pedigrees. *PLOS ONE* 8, e70151.
- Keough, K.C., Lyalina, S., Olvera, M.P., Whalen, S., Conklin, B.R., and Pollard, K.S. (2019). AlleleAnalyzer: a tool for personalized and allele-specific sgRNA design. *Genome Biol* 20, 1–9.
- Kleinstiver, B.P., Pattanayak, V., Prew, M.S., Tsai, S.Q., Nguyen, N.T., Zheng, Z., and Joung, J.K. (2016). High-fidelity CRISPR-Cas9 nucleases with no detectable genome-wide off-target effects. *Nature* 529, 490–495.
- Kohn, D.B., and Kuo, C.Y. (2017). New frontiers in the therapy of primary immunodeficiency: From gene addition to gene editing. *Journal of Allergy and Clinical Immunology* 139, 726–732.
- Kosicki, M., Tomberg, K., and Bradley, A. (2018). Repair of double-strand breaks induced by CRISPR-Cas9 leads to large deletions and complex rearrangements. *Nature Biotechnology* 36, 765–771.
- Lagarde, C., Hamel-Teillac, D., De Prost, Y., Blanche, S., Thomas, C., Fischer, A., Nordmann, Y., Ged, C., and De Verneuil, H. (1998). [Allogeneic bone marrow transplantation in congenital erythropoietic porphyria. Gunther's disease]. *Ann Dermatol Venereol* 125, 114–117.
- Li, X.-L., Li, G.-H., Fu, J., Fu, Y.-W., Zhang, L., Chen, W., Arakaki, C., Zhang, J.-P., Wen, W., Zhao, M., et al. (2018). Highly efficient genome editing via CRISPR-Cas9 in human pluripotent stem cells is achieved by transient BCL-XL overexpression. *Nucleic Acids Res* 46, 10195–10215.
- Li, Y., Zhang, Y., Li, X., Yi, S., and Xu, J. (2019). Gain-of-Function Mutations: An Emerging Advantage for Cancer Biology. *Trends in Biochemical Sciences* 44, 659–674.
- Liang, X., Potter, J., Kumar, S., Ravinder, N., and Chesnut, J.D. (2017). Enhanced CRISPR/Cas9-mediated precise genome editing by improved design and delivery of gRNA, Cas9 nuclease, and donor DNA. *Journal of Biotechnology* 241, 136–146.
- Liu, M., Rehman, S., Tang, X., Gu, K., Fan, Q., Chen, D., and Ma, W. (2019). Methodologies for Improving HDR Efficiency. *Front. Genet.* 9.
- Ma, H., Marti-Gutierrez, N., Park, S.-W., Wu, J., Lee, Y., Suzuki, K., Koski, A., Ji, D., Hayama, T., Ahmed, R., et al. (2017). Correction of a pathogenic gene mutation in human embryos. *Nature* 548, 413–419.
- Maruyama, T., Dougan, S.K., Truttmann, M.C., Bilate, A.M., Ingram, J.R., and Ploegh, H.L. (2015). Increasing the efficiency of precise genome editing with CRISPR-Cas9 by inhibition of nonhomologous end joining. *Nat Biotech* 33, 538–542.

- Molla, K.A., and Yang, Y. (2019). CRISPR/Cas-Mediated Base Editing: Technical Considerations and Practical Applications. *Trends in Biotechnology* 37, 1121–1142.
- Monteys, A.M., Ebanks, S.A., Keiser, M.S., and Davidson, B.L. (2017). CRISPR/Cas9 Editing of the Mutant Huntingtin Allele In Vitro and In Vivo. *Molecular Therapy* 25, 12–23.
- Morris, E.C., Fox, T., Chakraverty, R., Tendeiro, R., Snell, K., Rivat, C., Grace, S., Gilmour, K., Workman, S., Buckland, K., et al. (2017). Gene therapy for Wiskott-Aldrich syndrome in a severely affected adult. *Blood* 130, 1327–1335.
- Nambiar, T.S., Billon, P., Diedenhofen, G., Hayward, S.B., Tagliatela, A., Cai, K., Huang, J.-W., Leuzzi, G., Cuella-Martin, R., Palacios, A., et al. (2019). Stimulation of CRISPR-mediated homology-directed repair by an engineered RAD18 variant. *Nat Commun* 10, 1–13.
- Peinado, C.M., Heredia, C.D. de, To-Figueras, J., Arias-Santiago, S., Noguerras, P., Elorza, I., Olivé, T., Bádenas, C., Moreno, M.J., Tercedor, J., et al. (2013). Successful Treatment of Congenital Erythropoietic Porphyria Using Matched Unrelated Hematopoietic Stem Cell Transplantation. *Pediatric Dermatology* 30, 484–489.
- Porteus, M.H., and Baltimore, D. (2003). Chimeric Nucleases Stimulate Gene Targeting in Human Cells. *Science* 300, 763–763.
- Rabai, A., Reisser, L., Reina-San-Martin, B., Mamchaoui, K., Cowling, B.S., Nicot, A.-S., and Laporte, J. (2019). Allele-Specific CRISPR/Cas9 Correction of a Heterozygous DNMT3A Mutation Rescues Centronuclear Myopathy Cell Phenotypes. *Molecular Therapy - Nucleic Acids* 16, 246–256.
- Ribeil, J.-A., Hacein-Bey-Abina, S., Payen, E., Magnani, A., Semeraro, M., Magrin, E., Caccavelli, L., Neven, B., Bourget, P., El Nemer, W., et al. (2017). Gene Therapy in a Patient with Sickle Cell Disease. *N Engl J Med* 376, 848–855.
- Richard, E., Robert-Richard, E., Ged, C., and Verneuil, F.M.-G. and H. de (2008). Erythropoietic Porphyrias: Animal Models and Update in Gene-Based Therapies. *Curr. Gene Ther.* 8, 176-186
- Robert-Richard, E., Moreau-Gaudry, F., Lalanne, M., Lamrissi-Garcia, I., Cario-André, M., Guyonnet-Dupérat, V., Taine, L., Ged, C., and Verneuil, H. de (2008). Effective Gene Therapy of Mice with Congenital Erythropoietic Porphyria Is Facilitated by a Survival Advantage of Corrected Erythroid Cells. *The American Journal of Human Genetics* 82, 113–124.
- Saito, S., Maeda, R., and Adachi, N. (2017). Dual loss of human POLQ and LIG4 abolishes random integration. *Nat Commun* 8, 1–10.
- Shaw, P.H., Mancini, A.J., McConnell, J.P., Brown, D., and Kletzel, M. (2001). Treatment of congenital erythropoietic porphyria in children by allogeneic stem cell transplantation: a case report and review of the literature. *Bone Marrow Transplant* 27, 101–105.
- Shin, H.Y., Wang, C., Lee, H.K., Yoo, K.H., Zeng, X., Kuhns, T., Yang, C.M., Mohr, T., Liu, C., and Hennighausen, L. (2017). CRISPR/Cas9 targeting events cause complex deletions and insertions at 17 sites in the mouse genome. *Nat Commun* 8, 1–10.
- Slaymaker, I.M., Gao, L., Zetsche, B., Scott, D.A., Yan, W.X., and Zhang, F. (2016). Rationally engineered Cas9 nucleases with improved specificity. *Science* 351, 84–88.

Smith, C., Abalde-Atristain, L., He, C., Brodsky, B.R., Braunstein, E.M., Chaudhari, P., Jang, Y.-Y., Cheng, L., and Ye, Z. (2015). Efficient and Allele-Specific Genome Editing of Disease Loci in Human iPSCs. *Molecular Therapy* 23, 570–577.

Song, J., Yang, D., Xu, J., Zhu, T., Chen, Y.E., and Zhang, J. (2016). RS-1 enhances CRISPR/Cas9- and TALEN-mediated knock-in efficiency. *Nat Commun* 7, 1–7.

Takahashi, K., Tanabe, K., Ohnuki, M., Narita, M., Ichisaka, T., Tomoda, K., and Yamanaka, S. (2007). Induction of Pluripotent Stem Cells from Adult Human Fibroblasts by Defined Factors. *Cell* 131, 861–872.

Tezcan, I., Xu, W., Gurgey, A., Tuncer, M., Cetin, M., Öner, C., Yetgin, S., Ersoy, F., Aizencang, G., Astrin, K.H., et al. (1998). Congenital Erythropoietic Porphyria Successfully Treated by Allogeneic Bone Marrow Transplantation. *Blood* 92, 4053–4058.

Thomas, C., Ged, C., Nordmann, Y., Verneuil, H. de, Pellier, I., Fischer, A., and Blanche, S. (1996). Correction of congenital erythropoietic porphyria by bone marrow transplantation. *The Journal of Pediatrics* 129, 453–456.

Tsai, S., Bishop, D.F., and Desnick, R.J. (1987). Coupled-enzyme and direct assays for uroporphyrinogen III synthase activity in human erythrocytes and cultured lymphoblasts: Enzymatic diagnosis of heterozygotes and homozygotes with congenital erythropoietic porphyria. *Analytical Biochemistry* 166, 120–133.

Wang, H., Yang, H., Shivalila, C.S., Dawlaty, M.M., Cheng, A.W., Zhang, F., and Jaenisch, R. (2013). One-Step Generation of Mice Carrying Mutations in Multiple Genes by CRISPR/Cas-Mediated Genome Engineering. *Cell* 153, 910–918.

Xie, C., Zhang, Y.-P., Song, L., Luo, J., Qi, W., Hu, J., Lu, D., Yang, Z., Zhang, J., Xiao, J., et al. (2016). Genome editing with CRISPR/Cas9 in postnatal mice corrects PRKAG2 cardiac syndrome. *Cell Res* 26, 1099–1111.

Yamamoto, Y., Makiyama, T., Harita, T., Sasaki, K., Wuriyanghai, Y., Hayano, M., Nishiuchi, S., Kohjitani, H., Hirose, S., Chen, J., et al. (2017). Allele-specific ablation rescues electrophysiological abnormalities in a human iPS cell model of long-QT syndrome with a CALM2 mutation. *Hum Mol Genet* 26, 1670–1677.

Yang, L., Mali, P., Kim-Kiselak, C., and Church, G. (2014). CRISPR-Cas-Mediated Targeted Genome Editing in Human Cells. In *Gene Correction: Methods and Protocols*, F. Storici, ed. (Totowa, NJ: Humana Press), pp. 245–267.

Yasuda, M., and Desnick, R.J. (2019). Murine models of the human porphyrias: Contributions toward understanding disease pathogenesis and the development of new therapies. *Molecular Genetics and Metabolism* 128, 332–341.

Zelensky, A.N., Schimmel, J., Kool, H., Kanaar, R., and Tijsterman, M. (2017). Inactivation of Pol θ and C-NHEJ eliminates off-target integration of exogenous DNA. *Nat Commun* 8, 1–7.

Zhang, F., Cong, L., Lodato, S., Kosuri, S., Church, G.M., and Arlotta, P. (2011). Efficient construction of sequence-specific TAL effectors for modulating mammalian transcription. *Nat Biotechnol* 29, 149–153.

Zhang, J.-P., Li, X.-L., Li, G.-H., Chen, W., Arakaki, C., Botimer, G.D., Baylink, D., Zhang, L., Wen, W., Fu, Y.-W., et al. (2017). Efficient precise knockin with a double cut HDR donor after CRISPR/Cas9-mediated double-stranded DNA cleavage. *Genome Biol* 18, 1–18.

FIGURE LEGENDS:

Figure 1: CEP-hiPSC characterization

- A) CEP-hiPSC *UROS* genotyping. The CEP-hiPSC is composite heterozygous, with one allele mutated in exon 4 (c.217T>C) and the other one on the exon 10 (c.683C>T).
- B) WT-hiPSC and CEP-hiPSC *UROS* enzymatic activity. Quantification of *UROS* enzymatic activity by HPLC of WT or CEP-hiPSC. (Data are represented as mean \pm SEM. $n \geq 5$ independent experiments for each IPS cell lines).
- C) WT-hiPSC and CEP-hiPSC metabolic activity. Type I- fluorocytes accumulation (PE-Cy5-A) by flow cytometry: illustrative results of WT (top) and CEP-hiPSC (bottom) before and after δ -aminolevulinic acid (ALA) add (5mM, 12h).
- D) Experimental workflow for *UROS* gene editing and result analysis. CEP-hiPSC were transfected by nucleofection with a fluorescent ssODN template, a ZsGreen-nuclease plasmid and a RNA-guide plasmid targeting the exon 4 or 10. Then polyclonal and further monoclonal analysis were performed: HDR was quantified by RFLP, and confirmed by ICE and NGS. The Indels were quantified by ICE and NGS. The *UROS* functionality was assessed by quantifying *UROS*-specific activity by HPLC and type-I porphyrins accumulation by flow cytometry. For the subclones, chromosomal integrity was checked by FISH (analyze only performed for subclones).

Figure 2: Polyclonal analysis of *UROS* exon 10 editing by CRISPR-Cas9.

- A) (top) Schematic *UROS* locus on chromosome 10 with *UROS* gene overview and the exon 10 targeted region.
(Middle) Detailed view of exon 10 region close to c.683T mutation. CRISPR-mediated HDR design using a sgRNA targeting the sequence just next to the mutation (sgRNA-10 highlighted)

in blue) and a 75nt-ssODN-A647 carrying a silent restriction site *ApaI* (highlight in yellow) and the correction of the mutation (c.683C in red).

(Right) Scheme of *ApaI*-digested PCR products obtained for alleles with or without HDR and an illustrative RFLP analyze.

(Bottom) Exon 10 gene editing workflow. The CEP-hiPSC were transfected with a ZsGreen-nuclease plasmid, the sgRNA-10 plasmid and 75nt-ssODN-A647 template. The cells were sorted by cytometry to get back only the cells transfected with the ZsGreen-nuclease and the 75nt-ssODN-A647 template.

B) Flow cytometry illustration of the double positive ZsGreen⁺/A647⁺ sorted cells (left) and their targeting region analysis: Sanger sequence (top), ICE (middle) and RFLP (bottom).

Figure 3: Molecular and metabolic analysis of *UROS* exon 10 corrected cells

A) (Top left) Cytometry sorting of corrected cells, with disappearance of porphyrins after ALA exposure (5mM, 12h) (porph^{neg} cells, PE-Cy5-A⁻). (top right) CEP-hiPSC and porphyrin negative sorted cells exon 10 genotyping. The targeted mutation and its correction are highlight in red, and the inserted silent restriction site *ApaI* in yellow. (middle right) ICE analyze with the indels and HDR percentages. (Bottom right) RFLP analyze of the targeted region.

B) Quantification of *UROS* enzymatic activity in the sorted population. (Data are represented as mean \pm SEM. n \geq 4 independent experiments for each hiPSC cell lines).

C) Indels sequence and their contribution percentage given by ICE software.

Figure 4: *UROS* Exon 10-subclones genotyping.

A) Sanger sequence of 6 porphyrin-neg subclones. The corrected mutation is highlight in red and the silent-restriction site *ApaI* in yellow. HDR and indels analysis by RFLP and ICE are indicated.

B) *UROS* enzymatic activity of polyclonal porphyrin negative-sorted population and corrected subclones. (Data are represented as mean \pm SEM, ***p<0.001 vs CEP hiPSC cell lines, n \geq 4

independent experiments for CEP and polyclonal porphyrins negative (corrected) cell lines. n=6 corrected subclones).

Figure 5: Polyclonal analysis of *UROS* exon 4 editing by CRISPR-Cas9.

- A) (top) Schematic *UROS* locus on chromosome 10 with *UROS* gene overview and the targeted exon 4.
(Bottom) Detailed view of exon 4 region and CRISPR-mediated HDR design using c.217C-targeting sgRNA (sgRNA-4 highlighted in blue) and a 80nt-ssODN-A647 carrying a silent restriction site *SacI* (highlight in yellow) and the correction of the mutation (c.217T in red).
(Right) Scheme of *SacI*-digested PCR products obtained for alleles with or without HDR and an illustrative RFLP analyze.
- B) Flow cytometry illustration of the double positive *ZsGreen*⁺/*A647*⁺ sorted cells (top left) and their targeting region analysis: Sanger sequence (top), ICE (middle), NGS (bottom left) and RFLP (bottom).
- C) Indels sequence and their contribution percentage given by ICE software

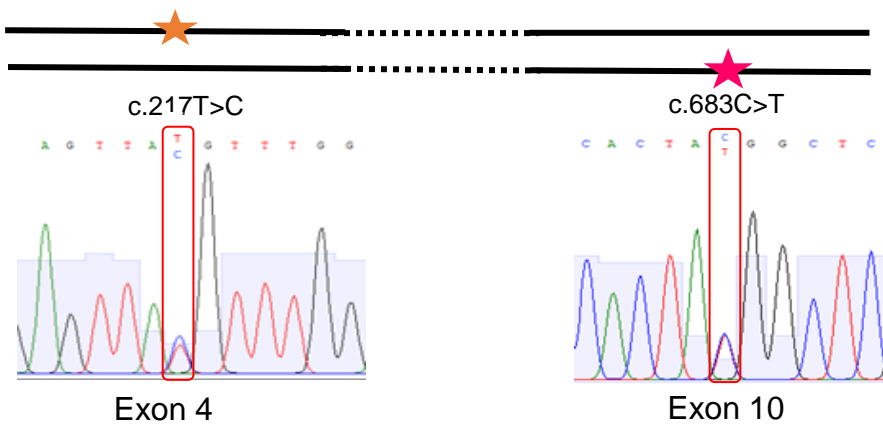
Figure 6: Molecular and metabolic analysis of *UROS* exon 4 corrected cells

- A) (Top left) Cytometry sorting of corrected cells, with disappearance of porphyrins after ALA exposure (5mM, 12h) (porph^{neg} cells, PE-Cy5-A⁻). (top right) CEP-hiPSC and porphyrin negative sorted cells exon 4 genotyping. The targeted mutation and its correction are highlight in red, and the inserted silent restriction site *SacI* in yellow. (middle right) ICE analyze with the indels and HDR percentages. (bottom right) RFLP analyze of the targeted region. (bottom left) NGS analyses of allelic outcome.
- B) Sequences and their contribution percentage given by ICE software
- C) Quantification of *UROS* enzymatic activity in the sorted population by HPLC. (Data are represented as mean \pm SEM, n \geq 6 independent experiments for each hiPSC cell line)

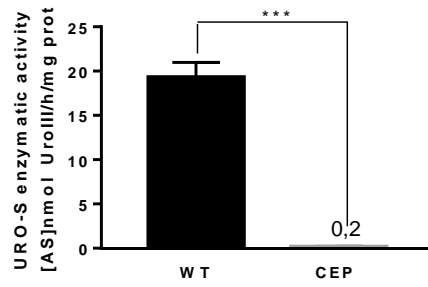
Figure 7: *UROS* Exon 4 subclones correction without karyotypic instability

- A) Exon-4 subclones genotyping. The corrected mutation is highlight in red and the silent-restriction site *SacI* in yellow. HDR and indels analysis by RFLP and ICE are indicated. Loq= limit of quantification 2%
- B) UROS enzymatic activity of polyclonal porphyrin neg-sorted population and 6 corrected subclones. (Data are represented as mean \pm SEM, * $p < 0.05$, ** $p < 0.01$ vs CEP hIPS cell lines, $n \geq 6$ independent experiments for CEP and polyclonal porphyrins negative (corrected) cell lines. $n = 6$ corrected subclones).
- C) DNA-FISH assay using *UROS*-framing probes (top) (-4.6Mb upstream and +4.4Mb downstream from *UROS* locus, respectively green (G) and Orange (O)). (bottom) Illustrative DNA-FISH results for the exon-4 subclones. (Magnification factor x630).
- D) Illustrative schema of a mutation-specific gRNA importance for heterozygous composite gene editing. The mutation is represented by blue cross, the gRNA by red line. The black dotted lines are the cut site of nuclease Cas9. Green dots represent the corrected mutation by HDR, and the red triangles are indels created by NHEJ repair of DSB.

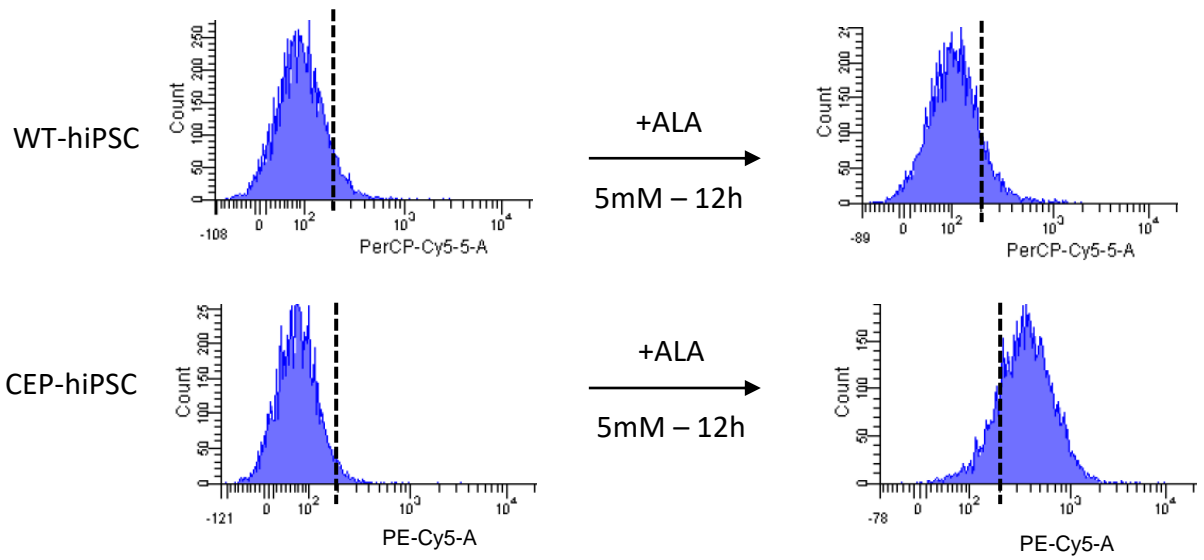
A



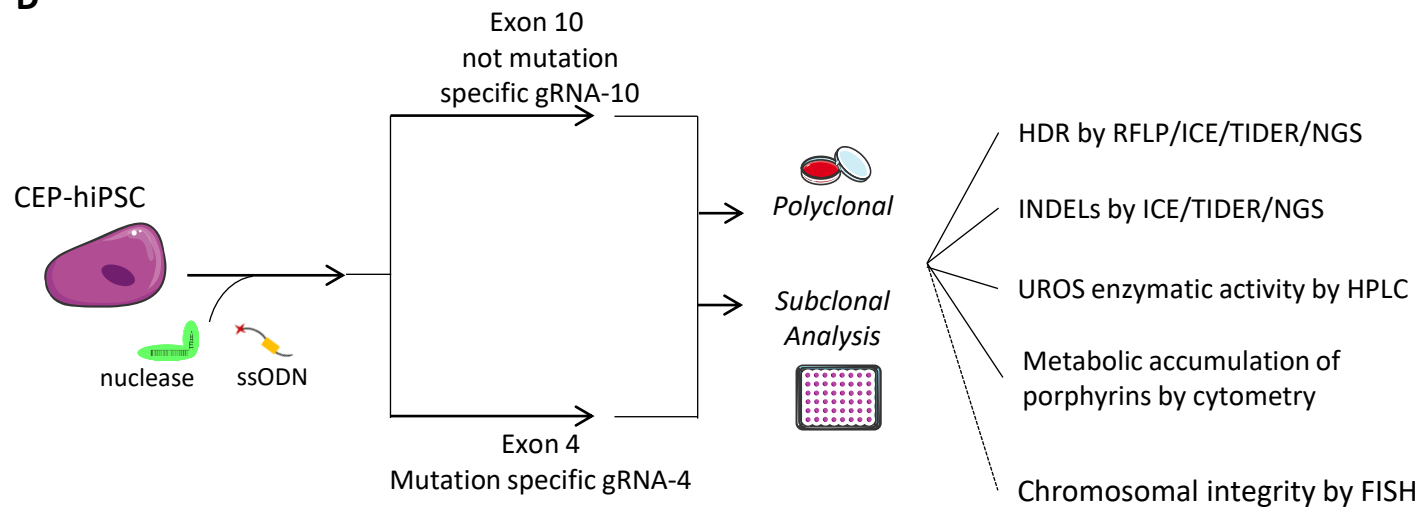
B

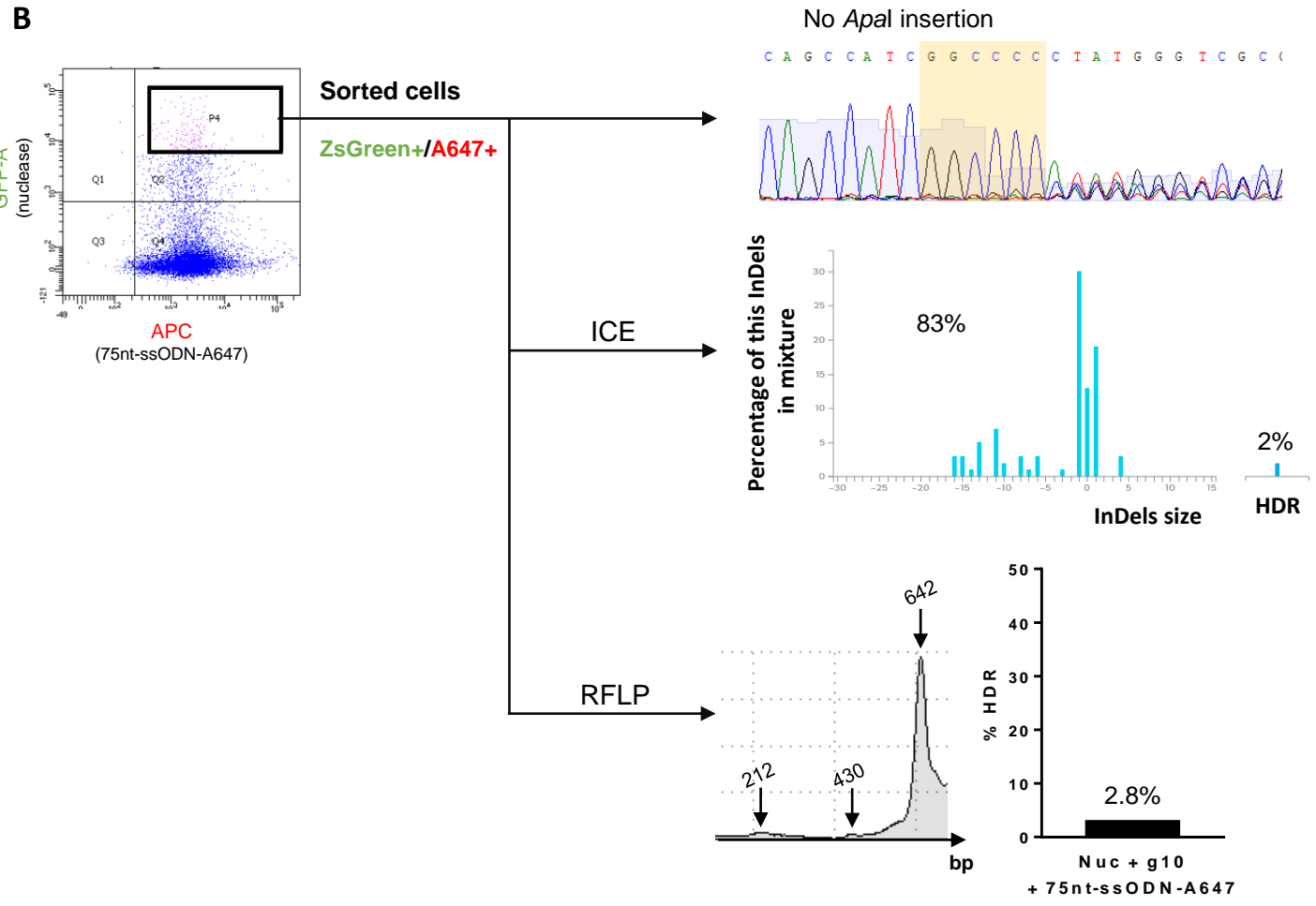
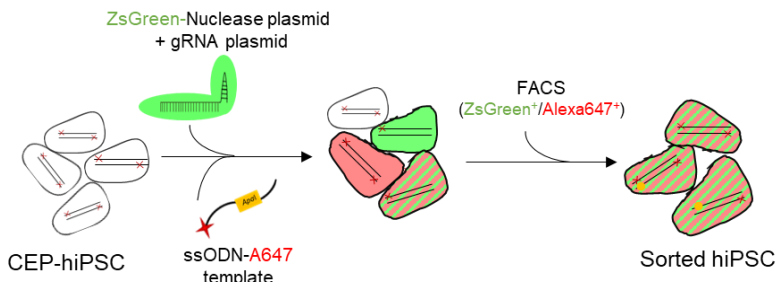
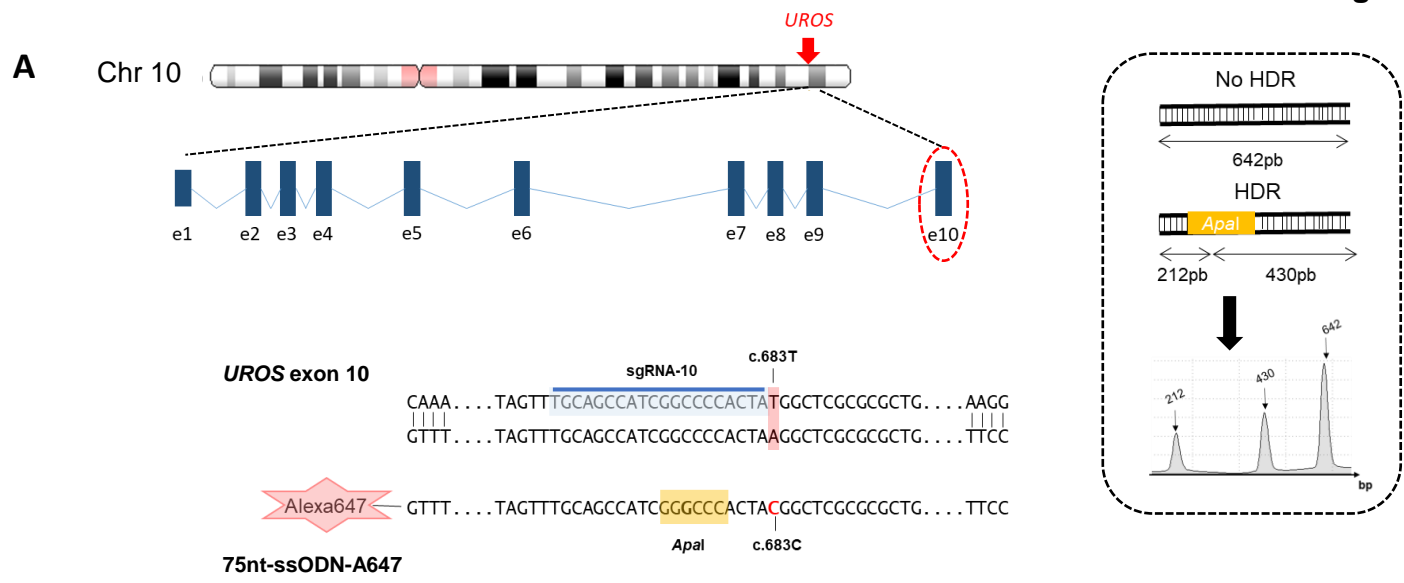


C

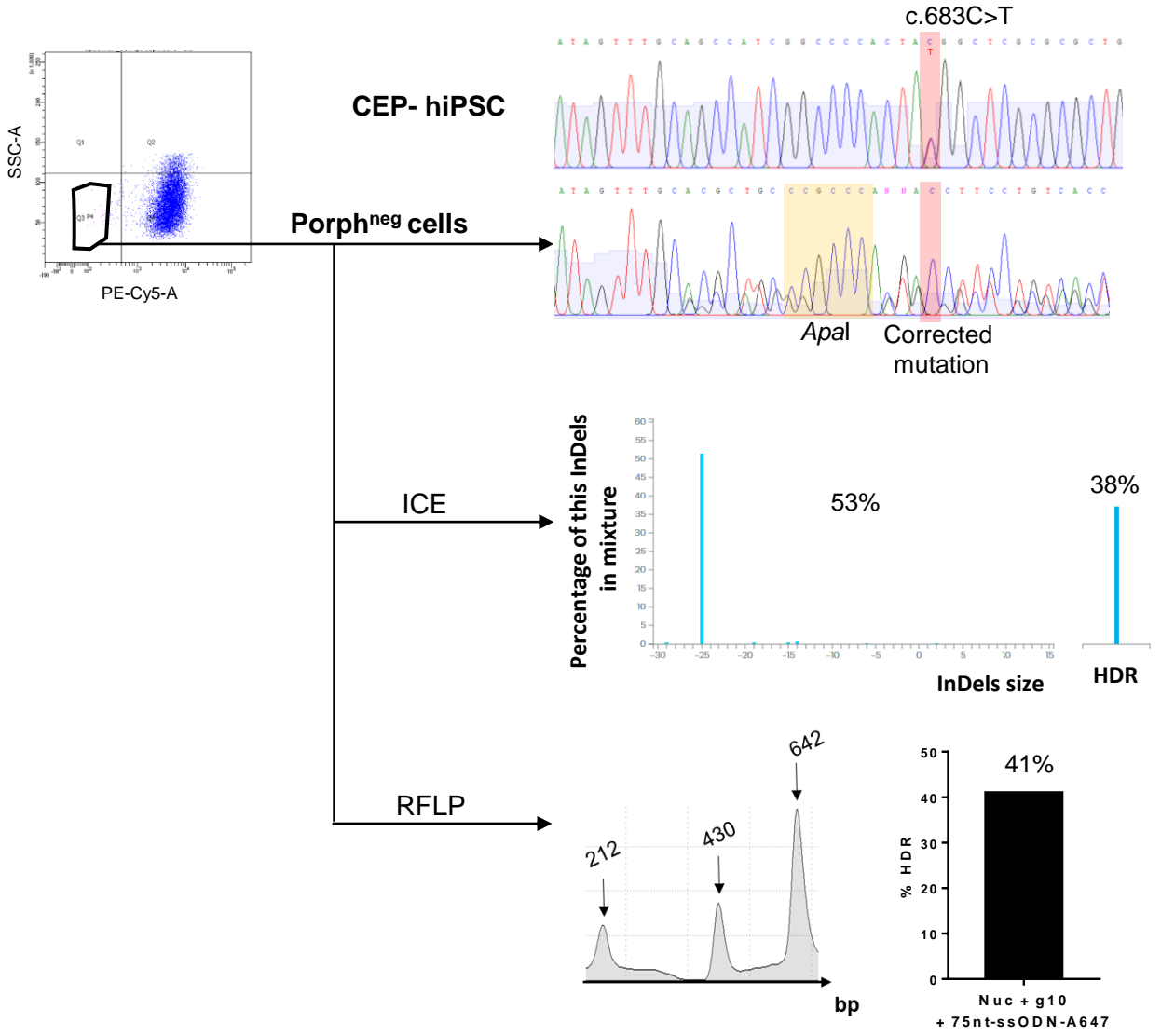


D

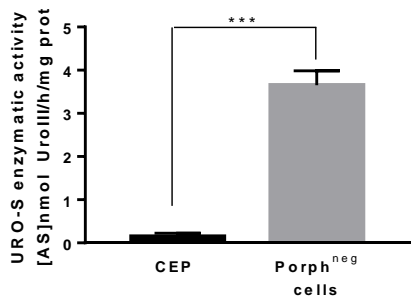




A

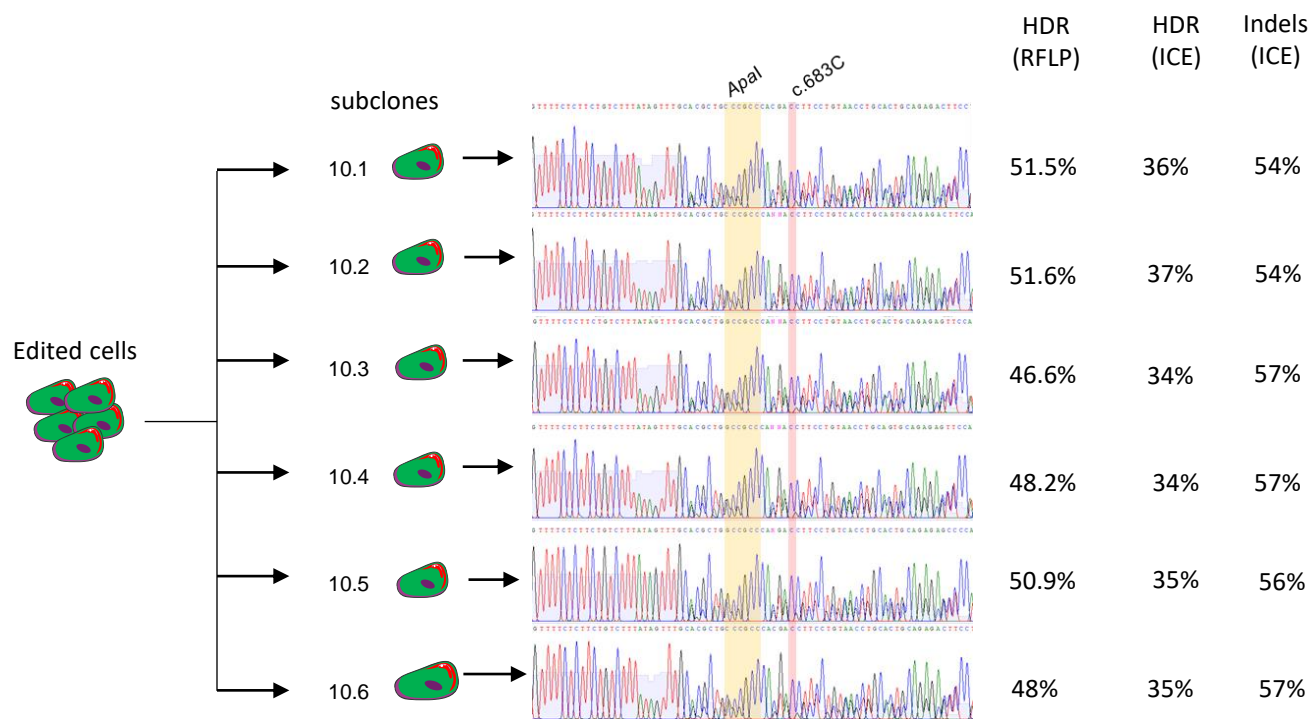
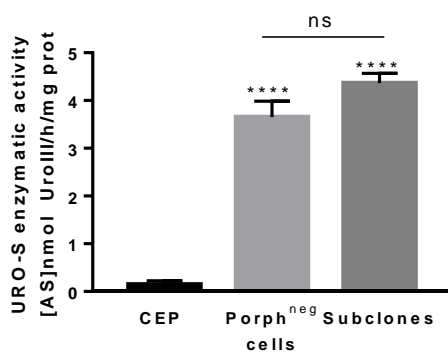


B

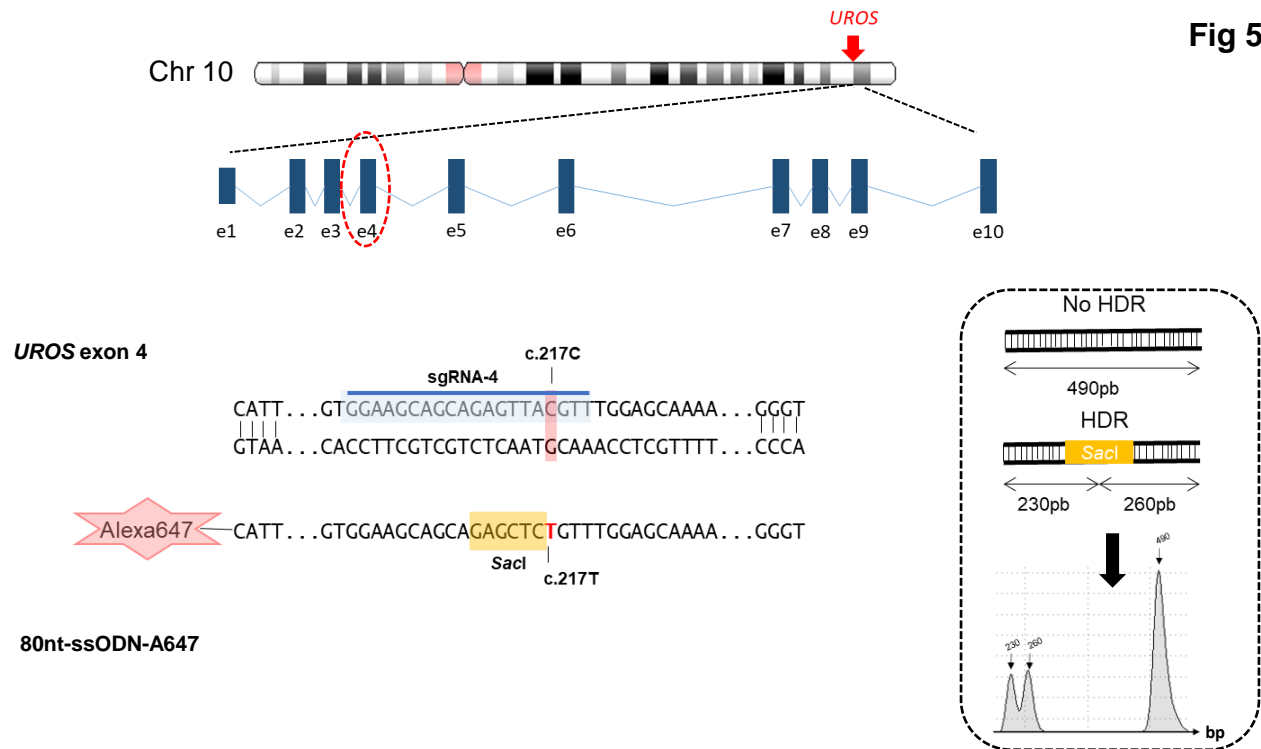


C

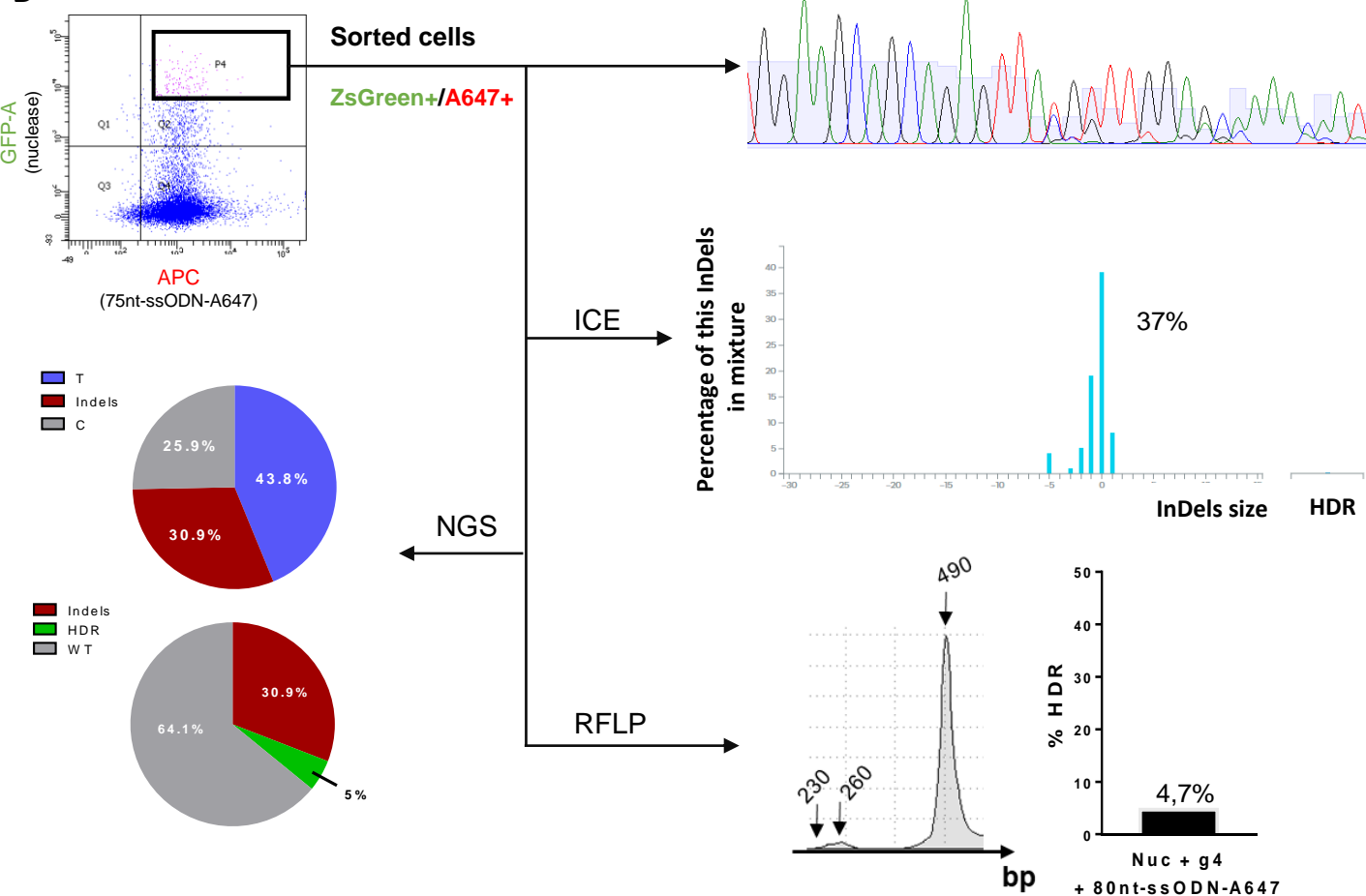
INDEL	CONTRIBUTION	SEQUENCE
HDR	37.1%	T T A T A G T T T G C A G C C A T C G G G C C C A C T A C G G C T C G C G C G C T G G C C G C C C A G G G C C T T C C T G T A A G C T G C A C T G C A
-25	26.3%	T T A T A G T T T G C - - - - - G C G T G G C G C C C A G G G C C T T C C T G T A A G C T G C A C T G C A
-25	24.9%	T T A T A G T T T G C A - - - - - C G T G G C C G C C C A G G G C C T T C C T G T A A G C T G C A C T G C A
-29	0.6%	T T A T A G T T T G C - - - - - T G G C G C C C A G G G C C T T C C T G T A A G C T G C A C T G C A
-15	0.6%	T T A T A G T T T G C A - - - - - A C G G C T C G C G C G C T G G C G C C C A G G G C C T T C C T G T A A G C T G C A C T G C A
-14	0.5%	T T A T A G T T T G C - - - - - C T A C G G C T C G C G C G C T G G C G C C C A G G G C C T T C C T G T A A G C T G C A C T G C A
-19	0.5%	T T A T A G T T T G - - - - - G G C T G G C G C G C T G G C G C C C A G G G C C T T C C T G T A A G C T G C A C T G C A
-6	0.3%	T T A T A G T T T G C A G C C A T C G - - - - - C T A C G G C T C G C G C G C T G G C C G C C C A G G G C C T T C C T G T A A G C T G C A C T G C A
-14	0.2%	T T A T A G T T T G C A - - - - - T A C G G C T C G C G C G C T G G C G C C C A G G G C C T T C C T G T A A G C T G C A C T G C A
+2	0.2%	T T A T A G T T T G C A G C C A T C G G C C C A N N C T A C G G C T C G C G C T G G C G C C C A G G G C C T T C C T G T A A G C T G C A C T G
-19	0.1%	T T A T A G T T T G C - - - - - G C T C G C G C G C T G G C G C C C A G G G C C T T C C T G T A A G C T G C A C T G C A
-10	0%	T T A T A G T T T G C A G C C A T C - - - - - C G G C T C G C G C G C T G G C G C C C A G G G C C T T C C T G T A A G C T G C A C T G C A
-16	0%	T T A T A G T T T G - - - - - T A C G G C T C G C G C G C T G G C G C C C A G G G C C T T C C T G T A A G C T G C A C T G C A

Fig 4**A****B**

A

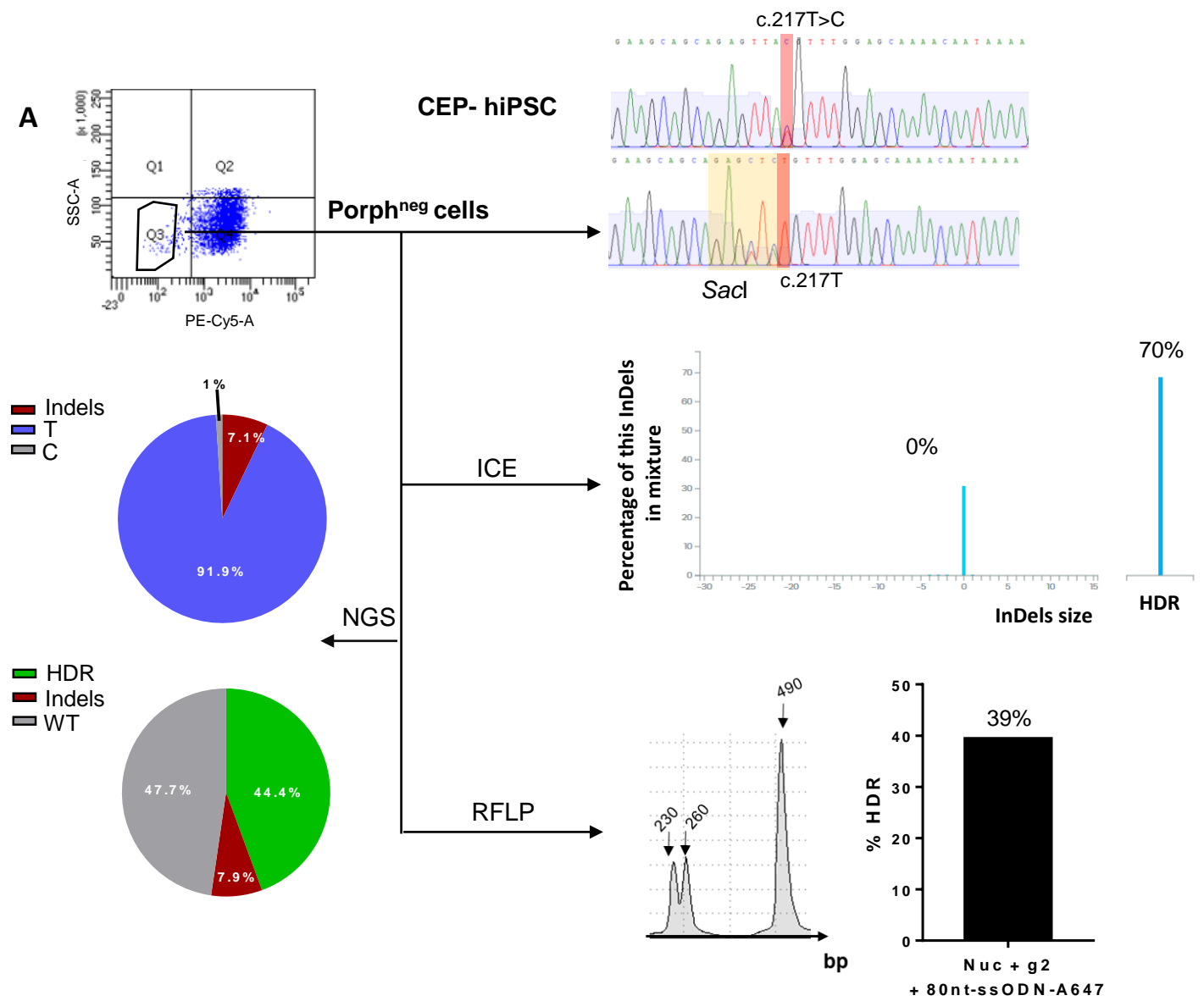


B



C

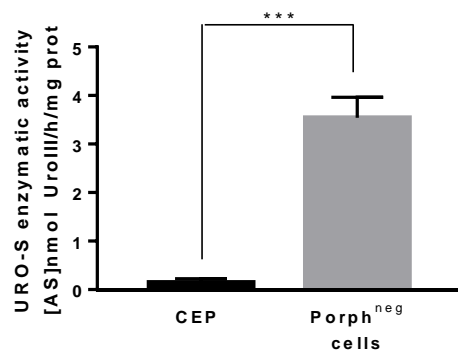
INDEL	CONTRIBUTION	SEQUENCE
0	39%	A G A G C A G T G G A A G C A G C A G A G T T A C G T T T G G A G C A A A A C A A T A A A A C T G A A G G T G A G G G T G G G T C T G C T G T G G A T
-1	18%	A G A G C A G T G G A A G C A G C A G A G T T A C - T T T G G A G C A A A A C A A T A A A A C T G A A G G T G A G G G T G G G T C T G C T G T G G A T
+1	8%	A G A G C A G T G G A A G C A G C A G A G T T A C N G T T T G G A G C A A A A C A A T A A A A C T G A A G G T G A G G G T G G G T C T G C T G T G G A
-2	5%	A G A G C A G T G G A A G C A G C A G A G T T A C - T T T G G A G C A A A A C A A T A A A A C T G A A G G T G A G G G T G G G T C T G C T G T G G A T
-5	4%	A G A G C A G T G G A A G C A G C A G A G T T A C - - - G A G C A A A A C A A T A A A A C T G A A G G T G A G G G T G G G T C T G C T G T G G A T
-3	1%	A G A G C A G T G G A A G C A G C A G A G T T A C - - T T T G G A G C A A A A C A A T A A A A C T G A A G G T G A G G G T G G G T C T G C T G T G G A T
-1	1%	A G A G C A G T G G A A G C A G C A G A G T T A C - G T T T G G A G C A A A A C A A T A A A A C T G A A G G T G A G G G T G G G T C T G C T G T G G A T

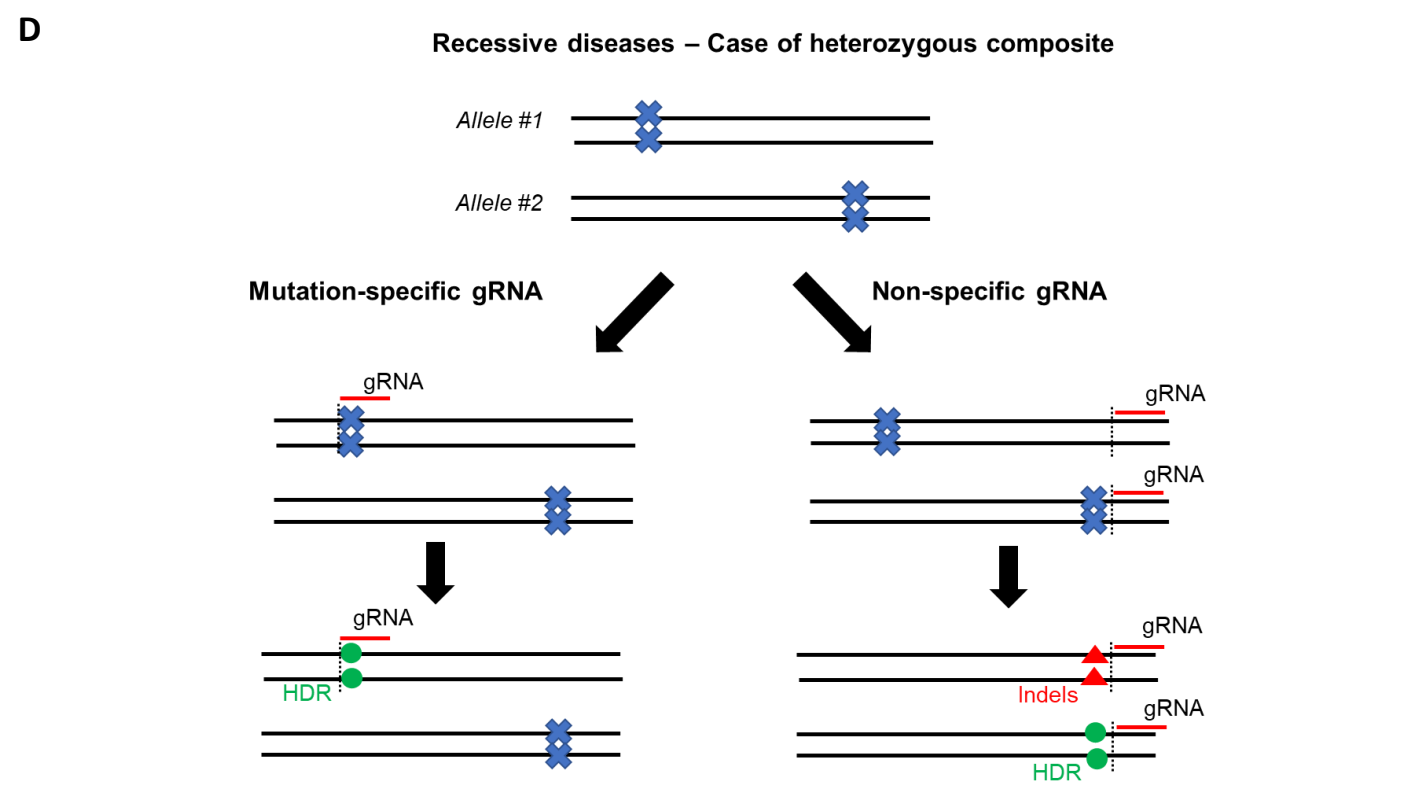
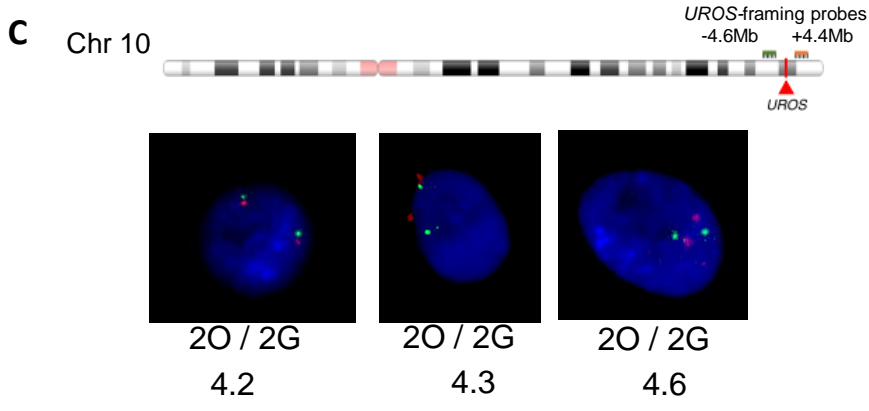
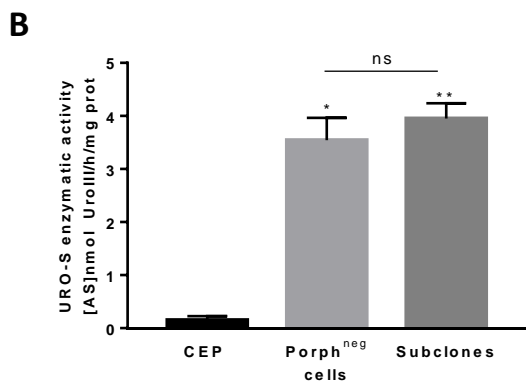
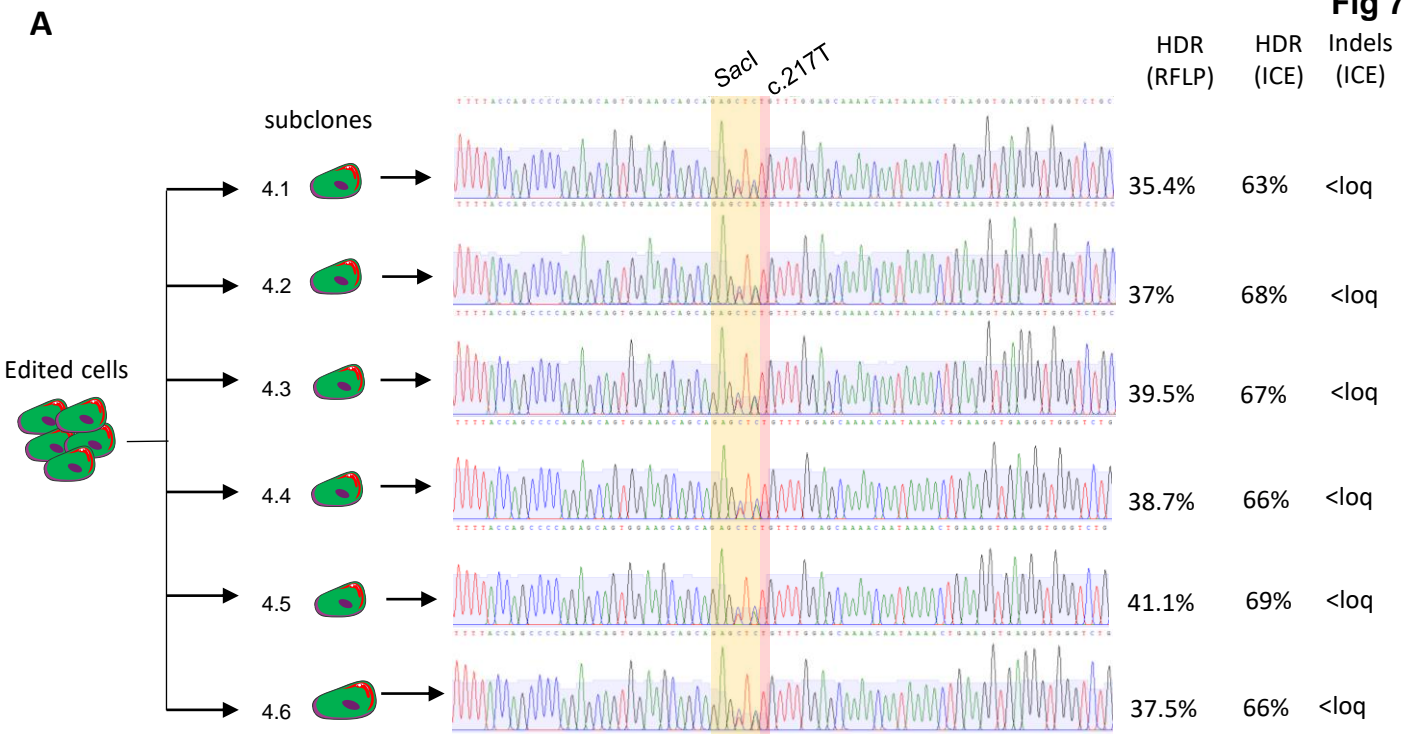


B

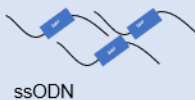
INDEL	CONTRIBUTION	SEQUENCE
HDR	70%	A G A G C A G T G G A A G C A G C A G A G C T C T G T T T G G A G C A A A A C A A T A A A A C T G A A G G T G A G G G T G G G T C T G C T G T G G A T
+	30%	A G A G C A G T G G A A G C A G C A G A G T T A C T G T T T G G A G C A A A A C A A T A A A A C T G A A G G T G A G G G T G G G T C T G C T G T G G A T

C

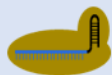




CEP-hiPSC



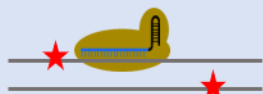
ssODN



Cas9

Near mutation

Encompassing mutation



Corrected hiPSC



Corrected hiPSC

